Soil Dynamics and Earthquake Engineering 197 (2025) 109459

Contents lists available at ScienceDirect

Soil Dynamics and Earthquake Engineering

journal homepage: www.elsevier.com/locate/soildyn

# Numerical simulations of seismic centrifuge tests: Validation of pore water pressure models in sand

Daniela Dominica Porcino [a,*], Giuseppe Tomasello [a], Daniela Giretti [b], Vincenzo Fioravante [c]

[a] University "Mediterranea" of Reggio Calabria – Department of Civil, Energy, Environmental and Material Engineering (DICEAM), Via Zehender (già Via Graziella), 89122, Reggio Calabria, Italy
[b] University of Bergamo – Department of Engineering and Applied Science, 24044, Bergamo, Italy
[c] University of Ferrara – Engineering Department, 44124, Ferrara, Italy

ARTICLE INFO

*Keywords:*
Clean sand
Centrifuge
Numerical analysis
Pore water pressure
Energy-based approach
Strain-based approach
Simple shear

ABSTRACT

A realistic prediction of excess pore water pressure generation and the onset of liquefaction during earthquakes are crucial when performing effective seismic site response analysis. In the present research, the validation of two pore water pressure (PWP) models, namely energy-based GMP and strain-based VD models implemented in a one-dimensional site response analysis code, was conducted by comparing numerical predictions with high-quality seismic centrifuge test measurements. A careful discussion on the selection of input soil parameters for numerical simulations was made with particular emphasis on the PWP model parameter calibration which was based on undrained stress-controlled/strain-controlled cyclic simple shear (CSS) tests carried out on the same sand used in the centrifuge test. The results of the study reveal that the energy-based model predicts at all depths peak pore water pressures and dissipation behaviour in a satisfactory way with respect to experimental measurements, whereas the strain-based model underestimates the PWP measurements at low depths. Further comparisons of the acceleration response spectra illustrate that both the strain- and energy-based models provide higher computed spectral accelerations near the ground surface compared with the recorded ones, whereas the agreement is reasonable at middle depth.

## 1. Introduction

The build-up of excess pore water pressure during strong earthquake shaking in saturated loose sandy soils may cause a severe reduction in strength and stiffness up to triggering of liquefaction and consequent serious damages to the built environment: building settlements, sand boils, ground cracks, landslides, dam instability, embankment failures or other hazards [1–4]. These damages are of great concern for public safety and their economic impact. Consequently, realistic predictions of liquefaction triggering and associated post-triggering phenomena/effects are complex engineering issues which have to be addressed and solved.

The residual excess pore water pressure $\Delta u_{res}$ (i.e. that one present when the applied shear stress is equal to zero) represents the main component resulting from the progressive collapse of the soil skeleton, namely plastic deformations, and thus it alters the effective stresses acting on the soil [5]. During the past 50 years, a number of methodologies were developed and proposed to predict the build-up of residual excess pore water pressures in clean sands, grouped under the categories of stress-based [6–9], strain-based [10–12], energy-based [13–17], plasticity theory-based [18–20] or others [21–23]. Limited studies concern sands with fines [24–29]. These models and the calibration parameters were developed based on extensive laboratory data from undrained cyclic stress- or strain-controlled tests, i.e. triaxial, simple shear or torsional shear tests as well [5,10,26,27,30,31]. Each of the above mentioned models has both advantages and limitations; a brief review of the different models is reported in section 2 with particular emphasis to those considered in the present study.

The validation of pore water pressure generation models is very important, but it is difficult to achieve from field case histories because: *a*) measurements of pore pressures generated and dissipated during real earthquakes are rather limited [32–34]; *b*) the in-situ soil conditions and input motion are seldom known with sufficient accuracy; *c*) installation of adequate instrumentation (i.e. piezometers and accelerometers) for

* Corresponding author.
*E-mail addresses:* daniela.porcino@unirc.it (D.D. Porcino), giuseppe.tomasello@unirc.it (G. Tomasello), daniela.giretti@unibg.it (D. Giretti), vincenzo.fioravante@unife.it (V. Fioravante).

https://doi.org/10.1016/j.soildyn.2025.109459
Received 14 January 2025; Received in revised form 11 April 2025; Accepted 16 April 2025
Available online 19 May 2025

continuous recording of relevant parameters during seismic events are required. For this reason, artificial generation of liquefaction in the field (e.g. blasting [35–37], or physical modeling, e.g. shaking tables [38–40] or centrifuge tests [41–45]) are generally adopted to obtain high-quality pore water pressure and acceleration measurements. Among model tests which can be conducted in the laboratory under controlled conditions, dynamic centrifuge tests utilise a high acceleration field preserving the stress-strain response of the prototype soil, thus providing accurate and reliable measures of excess pore pressure build-up and onset of liquefaction. In this context, comparisons between numerical simulations and experimental measurements in centrifuge experiments demonstrate the pronounced differences in the accuracies of pore pressure model predictions of soil subjected to a transient earthquake loading. Dobry et al. [44] presented numerical predictions of excess pore pressure, liquefaction and settlement response of four centrifuge model tests performed on saturated clean Ottawa sand having a relative density ranging from 38 % to 66 %. The deposits were subjected to 1D uniform base shaking consisting of 10–15 cycles of peak acceleration. The experimental and numerical results showed that both cyclic shear stress/strains and upward water flow determine together the pore pressure build-up and liquefaction phenomena. The soil response is partially drained rather than undrained, and pore pressure dissipation does take place during shaking both before and after liquefaction occurs. Moreover, a careful and realistic selection of the input soil parameters in the numerical simulations, such as compressibility and permeability, are crucial for capturing in a realistic way the experimental measurements in terms of excess pore pressure and settlement time histories. Changes in the effective (interconnected) porosity of the soil mass and tortuosity of the flow paths through the porous medium have the main roles in altering the permeability of the saturated sand during earthquake loading [46]. Several experimental studies evidenced an "average" increase of the permeability coefficient $k$ during cyclic loading as high as 4–10 times the initial (static) value [46–51]. The assumption of a variable permeability function in numerical models was shown to capture in a satisfactory way the response measured in centrifuge tests in terms of excess pore pressure time histories at different depths and settlements of ground surface as well [46,49].

Recently, Pervaiz et al. [52] used centrifuge tests on mildly sloping ground subjected to ramped sinewaves to investigate the performance of three seismic pore pressure models, based on accumulated strain, energy and stress, implemented in a one-dimensional (1D) site response analysis program. One-dimensional effective stress site response analyses are run more frequently than two- (2D) and three-dimensional (3D) simulations in engineering practice to develop site-specific free-field ground motions [44,52].

This paper presents comprehensive numerical simulations of dynamic centrifuge tests through non-linear 1D seismic site response analysis conducted by DEEPSOIL code [53]. A numerical procedure is used to predict both generation and dissipation of excess pore water pressures of sand to verify the reliability of two PWP models capable of taking into account the developed strains during seismic events, namely strain-based VD model [11] and energy-based GMP model [14] both implemented in DEEPSOIL [53].

For this purpose, undrained cyclic simple shear (CSS) tests were carried out on the same material used in centrifuge tests (Ticino sand), and the results were used for the calibration of model parameters essential to perform non-linear effective stress 1D analyses. The influence of permeability coefficient (and thus consolidation coefficient) was analysed to verify the sensitivity of the considered models to the changes of $k$ coefficient. Numerical predictions of excess pore pressure, liquefaction response and acceleration time histories of saturated Ticino sand at different depths were compared with centrifuge test experiments. If empirical PWP correlations developed from cyclic simple shear test data are used, the fit between predicted vs. measured values is expected to be improved [52].

This paper is part of an ongoing Research Project titled: "*SAFEGUARDING AND ENHANCING THE NATURAL AND CULTURAL HERITAGE AND IDENTITY OF THE TERRITORIES - TECHNOLOGIES FOR RESILIENT AND ACCESSIBLE CULTURAL AND NATURAL HERITAGE*" involving University Mediterranea of Reggio Calabria. Evaluation of seismic liquefaction hazard for structural and environmental safety of cultural heritage (settlements and historic buildings) in transition scenarios was one of the goals of the action 3 of the pilot project, as liquefaction vulnerability of soils in coastal areas may be amplified by the sea-level rising consequent to climate changes. For this reason, it is necessary to adopt mitigation strategies to reduce the risk of liquefaction.

Seismic centrifuge tests were performed in the context of the *LIQUEFACT* research project involving University of Ferrara, among others.

## 2. Overview of PWP build-up models under undrained cyclic loading

The well-known empirical stress-based models (StressBM) proposed firstly by Seed et al. [6] and afterwards by Booker et al. [7] consider that the residual excess PWP ratio ($R_{u,res}$) is strictly related to the normalised number of applied cycles ($N/N_f$), where $R_{u,res} = \Delta u_{res}/\sigma'_0$ is the ratio between the residual excess pore pressure, $\Delta u_{res}$, and the initial effective stress, $\sigma'_0$ (vertical stress in cyclic simple shear or mean effective stress in different conditions) and $N_f$ (one of the two calibration parameters) represents the number of cycles required to cause full liquefaction in the soil. The advantages of using the StressBM to predict excess pore water pressure due to a seismic event are [5,12]: *i*) the stress-based models are relatively simple and widely used for cyclic excess pore water pressure evaluation; *ii*) they are based on stress-controlled cyclic tests where the attained shear strain levels are higher than 1 % and therefore compatible with high shear strains associated with significant pore water pressure build-up. On the other hand, there are some disadvantages in using StressBM, such as: *i*) the difficulty in defining and estimating $N_f$, *ii*) a lack of effective differentiation between cyclic mobility and plastic strain accumulation responses of the soil, the second typical of sloping ground conditions; *iii*) earthquake motion has to be converted to an equivalent number of uniform cycles for the implementation of stress-based models in seismic site response analysis codes.

On this regard, an innovative category of stress-based models for sandy materials, i.e. the "damage parameter" models (DBM), were introduced to solve this last issue [25,54–57]. For sandy soils with low fines contents (i.e. <35 %), the following equation based on the model proposed by Seed et al. [6] is adopted [54]:

$$R_{u,res} = \frac{2}{\pi}\cdot\sin^{-1}\left(\frac{D}{D_f}\right)^{1/2\theta} \quad (1)$$

where $D$ is the damage parameter, $D_f$ is the damage parameter at liquefaction, and $\theta$ is a fitting parameter of the model. A value of $\theta = 0.7$ is recommended by Booker et al. [7] for clean sands. If the term $(D/D_f)$ of Eq. (1) was replaced by $(N/N_f)$, the relationship proposed by Seed et al. [6] can be obtained.

The damage parameter is defined as follows:

$$D = (\eta / CSR)\cdot(CSR - CSR_t)^{\delta} \quad (2)$$

where $CSR$ is the shear stress ratio (shear stress normalised to initial effective vertical stress), $CSR_t$ is the threshold shear stress ratio, below which no pore pressure rise can occur, $\eta$ is the length of the stress-path induced by seismic motion in the time domain and $\delta$ is a curve fitting parameter.

The variable $\eta$ in Eq. (2) is defined as [Eq. (3)]:

$$\eta = \int \frac{|d\tau|}{\sigma'_{v0}} \quad (3)$$

where $\tau$ is the shear stress induced by seismic motion in the time domain.

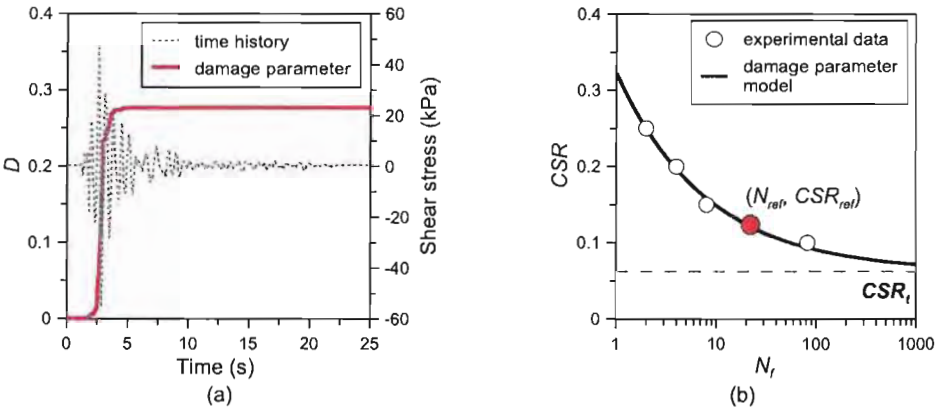


**Fig. 1.** – Illustrative representation of damage-based model parameter: (a) trend of damage parameter $D$ with time for irregular shear stress history, (b) cyclic resistance curve.

Consequently, the damage parameter is an incremental quantity that accumulates at each time step of an irregular shear stress history (Fig. 1a) without the need of converting it to an equivalent shear stress history. In a stress-controlled cyclic loading, $\eta$ simplifies to $4{\cdot}N{\cdot}CSR$. Therefore, the damage parameter at failure (liquefaction) for cyclic tests is expressed by Eq. (4):

$$D_f = 4{\cdot}N_f{\cdot}(CSR - CSR_t)^{\delta} \tag{4}$$

The damage parameter model requires only the knowledge of the cyclic resistance curve of the soil (Fig. 1b). Specifically, the empirical parameter $CSR_t$ represents the horizontal asymptote of cyclic liquefaction curve, while the curve fitting parameter $\delta$ defines the slope of the cyclic resistance curve in the logarithmic plane (Fig. 1b). The parameter $\delta$ can be determined through a trial and error fitting procedure applied to the equation of liquefaction curve [Eq. (5)]. This equation, derived combining Eqs. (2) and (4), is the following:

$$\left(\frac{CSR - CSR_t}{CSR_{ref} - CSR_t}\right)^{\delta} = \left(\frac{N_{ref}}{N}\right) \tag{5}$$

where $CSR_{ref}$ is the $CSR$ value at a reference number of loading cycles ($N_{ref}$). The selection of ($N_{ref}$, $CSR_{ref}$) point can be arbitrary.

As for the selection of the parameters $\theta$, $CSR_t$, and $\delta$, useful correlations relating these calibration parameters to the different influencing factors, such as relative density ($D_R$), cyclic stress ratio ($CSR$), mean grain size ($D_{50}$), fines content ($f_c$) for sands with non plastic fines less than 35 % was proposed by Porcino et al. [25] and Polito et al. [5]. In the case of silty sands with percentages of fines higher than 35 %, Eq. (1) has some restrictions and thus proposals of modification were made [25,56]. Although some studies were conducted in the literature to verify the performance of damage-based models through real case studies [57], model tests [52] or laboratory experimental investigation [56], definitive conclusions can not be reached yet.

Another category of PWP models is that based on strain (StrainBM) which considers that excess pore water pressure ratio ($R_u$) is strictly related to the cyclic shear strain ($\gamma$) due to the seismic event. The advantages of using strain-based models to predict excess pore water pressure due to a seismic event are [5,12,30]: *a*) the StrainBM are implemented in many effective-stress-based non-linear ground response modeling software, namely DESRA-2 [58], D-MOD2000 [59], and DEEPSOIL [53]; *b*) the StrainBM PWP relationship is relatively independent of the initial state (relative density, $D_R$) and cyclic applied stress ratio ($CSR$). On the other hand, some limitations are: *a*) implementation of strain-based models in earthquake site response analyses requires that the earthquake motion be converted to an equivalent number of uniform cycles; b) lack of effective differentiation between cyclic mobility and plastic strain accumulation responses relevant under sloping ground conditions; c) these models are generally based on strain-controlled cyclic tests which are not reliably able to test specimens at larger strain levels (>1 %).

The cyclic-strain based approach was originally developed by Dobry et al. [10] for sands based on the results of strain-controlled triaxial and simple shear tests and subsequently modified by Vucetic and Dobry [11], as follows:

$$R_u = \frac{p{\cdot}f{\cdot}N{\cdot}F{\cdot}(\gamma_c - \gamma_{tv})^s}{1 + f{\cdot}N{\cdot}F{\cdot}(\gamma_c - \gamma_{tv})^s} \tag{6}$$

where $\gamma_c$ = cyclic shear strain, $\gamma_{tv}$ = volumetric threshold shear strain below which there is no excess pore water pressure generation ($\gamma_{tv}$ is in the range 0.01 %–0.02 % for most soils [60]) and $N$ = number of loading cycles. Model parameter $f$ is set to 1 or 2 depending on whether pore pressures are induced by one- or two-directional shaking, whereas the parameters $p$, $F$, and $s$ are curve-fitting parameters depending on grain-size distribution and void ratio of sand.

Selection of the four curve fitting parameters of the model proposed by Vucetic and Dobry [11] (in the following termed as VD model) is crucial; useful recommendations were derived especially from laboratory experimental investigation performed by different researchers, such as Mei et al. [30], Matasović [61], Mei et al. [62] among the others. In particular, Mei et al. [62] proposed empirical correlations to select the StrainBM parameters based on an extensive database of 92 stress- and strain-controlled cyclic simple shear and cyclic triaxial (CTX) tests. In the present research, undrained cyclic stress- and strain-controlled constant volume simple shear tests were used to calibrate StrainBM for Ticino sand basing on Eq. (6). Additionally, a constant $\gamma_{tv} = 0.01$ % was used in all DEEPSOIL simulations performed in the present study.

Although the strain-based model was proved to reasonably predict the pore pressure build-up for the Wildlife liquefaction array case study [63] and centrifuge model tests [44,64], in some cases an underestimation of pore water pressures was found with respect to the experimentally measured values in centrifuge tests [52,65].

As an alternative to stress- and strain-based models, the energy-based approach (EBM) considers that $R_u$ is strictly related to seismic energy per unit volume ($W$) dissipated up to the considered stage of the cyclic history, i.e. $R_u = f(W)$. $W$ is computed by integrating the area bounded by hysteresis stress–strain loops of the soil subjected to a seismic loading. For granular soils, the dominant mechanism of energy dissipation is the frictional sliding at grain-to-grain contact surfaces [66].

The common basis of energy-based liquefaction evaluation methods (EBM) so far proposed is to compare energy capacity for liquefaction ($W_f$) with energy demand of design earthquakes, similar to the currently

employed stress-based method (StressBM). The energy capacity for liquefaction ($W_f$) corresponds to dissipated energy needed to trigger liquefaction condition during seismic loading according to the selected criterion.

Energy-based pore pressure models have received remarkable attraction because they offer several benefits with respect to StressBM and StrainBM approaches, such as: *a*) the conversion of earthquake motions to equivalent uniform cycles is not necessary [57]; *b)* the EBM can simultaneously consider the effect of stress and strain time histories on the liquefaction behaviour of soil; *c*) there is a unique relationship between PWP generation and dissipated energy, regardless of the stress-strain path and loading shape in each test [5,68–73]; *d*) EBMs are characterised by a simple formulation, facilitating their implementation in numerical modeling for assessing the pore pressure generation during earthquakes. Energy-based approach was adopted by numerous researchers performing cyclic triaxial tests [5,72,74–77], cyclic simple shear tests [16,28,31] and torsional shear as well [15,68,78,79]. Jafarian et al. [15] presented a summary of the previously published energy-based pore water pressure models evidencing the need to take into account the influence of parameters such as initial relative density, effective vertical stress, initial static shear stress. In the cyclic simple shear (CSS) tests, dissipated energy $W$ can be determined using the trapezoidal rule, by the following equation [Eq. (7)]:

$$W = \frac{1}{2}\sum_{i=1}^{n-1}(\tau_{i+1} + \tau_i)\cdot(\gamma_{i+1} - \gamma_i) \tag{7}$$

where $n$ = number of load increments, $\tau_{i+1}$ and $\tau_i$ are the applied shear stress at load increment i+1 and i, respectively, whereas $\gamma_{i+1}$ and $\gamma_i$ are the shear strains at load increment $i+1$ and $i$, respectively.

In particular, Berrill and Davis [13] proposed a simple expression:

$$R_u = \alpha \cdot W_n^{\beta} \tag{8}$$

where $W_n$ is the dissipated energy per unit volume of soil normalised to the initial mean effective stress $\sigma'_0$, and $\alpha$ and $\beta$ are two curve-fitting parameters to be determined by undrained cyclic tests. The proposed equation was developed based on undrained cyclic stress-controlled test data.

Another well-known energy-based PWP model proposed in the literature was the GMP model [14], which represents a special case of the more general Berrill and Davis [13] model. It can be expressed through the following relationship:

$$R_u = \sqrt{W_n/PEC} \leq 1 \tag{9}$$

where the calibration parameter *PEC* (dimensionless) is the pseudo energy capacity of the model. The illustration of how *PEC* is determined from cyclic test data is shown in the paragraph 3.3.2.1.

The GMP model was developed using data from tests performed on non plastic silt-sand mixtures that ranged in fines contents from clean sands to pure silts. It is worth mentioning that the stress-normalised $W$ (i.e. $W_n$) is introduced to unify the $R_u$-$W$ response of soil specimens, regardless of initial effective confining stress applied before cyclic loading.

Both models [Eqs. (8) and (9)] are implemented in 1D non-linear code DEEPSOIL [53]. Since the GMP model is characterised by only one calibration parameter, it will be adopted in the present study in the numerical analyses.

Validation of EBMs to explore their predictive capability by centrifuge test results was made by several authors, namely Jafarian et al. [15], Khashila et al. [17], Pervaiz et al. [52], Mei et al. [80]. It was found that numerical simulations by using the GMP energy-based model underestimated the pore pressures with respect to centrifuge test data [52,80]. On the other hand, other researchers, i.e. Khashila et al. [17], demonstrated that the generated pore pressure curves in centrifuge model tests on dense and loose Ottawa sand at different depths can successfully be compared with their counterparts obtained using the numerical simulations where a specifically proposed energy-based pore pressure model was incorporated by the authors. Basing on shaking table data and centrifuge test measurements conducted on clean sands (Toyoura sand and Nevada sand) to simulate level and mildly sloping ground sites, Jafarian et al. [15] observed a reasonable consistency between the measured and predicted curves of $R_u$-$W/W_f$ when an energy-based PWP model proposed by the authors was adopted.

Despite these developments, the contradictory findings gathered in the literature on the predictive capacity of different PWP generation models (stress, strain, energy) evidence the need for further research to compare experimental (centrifuge model tests) vs. predicted (numerical simulations) pore water pressure build-up in liquefied and not liquefied soils by applying real earthquakes, testing various soils of different densities and selecting appropriately all input data for numerical modeling. Additionally, high-quality laboratory tests by using apparatus which reflect the field loading conditions before and during earthquakes are necessary to derive the model calibration parameters in a reliable way.

## 3. Experimental program

### 3.1. Material properties

Both centrifuge tests and undrained cyclic simple shear tests for the calibration of excess pore water pressure models in this study were performed on Ticino sand, herein referred to as TS, a natural quartz sand whose particle-size distribution is presented in Fig. 2. The main physical, mechanical and hydraulic properties of the sand used in these tests are presented in Table 1.

TS was well characterised to derive input parameters of numerical analyses by oedometer tests, bender element tests in triaxial apparatus, resonant column tests and undrained cyclic simple shear tests as described in sections 3.3 and 4.1.

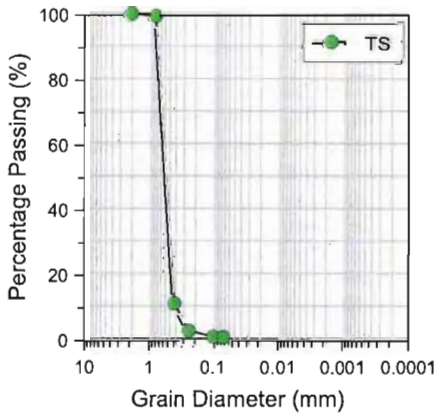


**Fig. 2.** – Grain size distribution curve of Ticino sand.

**Table 1**
– Physical, mechanical and hydraulic properties of Ticino sand.

| Parameter | Unit | Value |
|---|---|---|
| Minimum dry density, $\gamma_{d,min}$ | (kN/m$^3$) | 13.64 |
| Maximum dry density, $\gamma_{d,max}$ | (kN/m$^3$) | 16.67 |
| Specific gravity, $G_s$ | | 2.68 |
| Mean grain size, $D_{50}$ | (mm) | 0.57 |
| Critical state friction angle, $\varphi'_{cs}$ | (°) | 34 |
| Hydraulic conductivity, $k^a$ | (m/s) | $2{\cdot}10^{-3}$ |

[a] Value at the nominal void ratio of the centrifuge tests.

### 3.2. Seismic centrifuge model

The test here discussed was carried out in the framework of the LIQUEFACT project (http://www.liquefact.eu/, Giretti and Fioravante [45], Fioravante et al. [51]) at ISMGEO laboratory in Italy, and, as shown in Fig. 3a, it simulated a level ground, homogeneous, sandy deposit, 12.5 m deep, with the groundwater table at the soil surface. A geometrical scaling factor equal to 50 was adopted and the centrifugal acceleration of 50 g was imposed at the base of the model, g being the earth gravity.

The model was reconstituted using TS, dry pluviated at 1 g in an equivalent shear beam box [81,82], and it was saturated under vacuum using a solution of water and hydroxypropyl methylcellulose (HPMC). The sandy layer, once consolidated inflight, had a relative density of 47 %. Fig. 3a shows the position of the sensors at 1 g after reconstitution. As depicted in Fig. 3a, the model was instrumented with miniaturized accelerometers (acc), pore pressure transducers (ppt) and displacement transducers (D) to measure horizontal accelerations along the shaking direction, fluid pressures and settlements, respectively. The sensors embedded in the sand were located during the pluviation along the mid-section of the model. Accelerometer acc1 was fixed to the container base and it measured the applied seismic excitation.

The time history of the ground motion, applied to the model by the one DoF shaking table installed in the ISMGEO centrifuge, is shown in Fig. 3b at the prototype scale. The motion is characterised by a peak ground acceleration PGA = 0.215 g, significant duration $d_{90}$ = 15.09 s, an Arias Intensity $I_{A,max}$ = 0.348 m/s, the energy content concentrated at frequency higher than 1 Hz. The vertical lines in Fig. 3b indicate the time instants at which 5 % and 95 % of the Arias Intensity was released.

Fig. 4 shows the accelerations recorded at three relevant depths by the accelerometers, while Fig. 5 shows the excess pore pressure (Fig. 5a) and the pore pressure ratio $R_u$ (Fig. 5b) measured by the ppts. It is worth noting that the depth of the sensors indicated in Figs. 4 and 5 refers to their pre-shock location, attained after the inflight consolidation that the saturated sandy layer underwent at 50 g; this depth was estimated on the base of the superficial settlements recorded during the consolidation phase.

During the seismic excitation, all ppts recorded a peak excess pore water pressure value almost simultaneously in the first 12 s, higher at the base and decreasing upward. A max $R_u$ value equal to 0.7 was measured by ppt5, the shallower of the sensor array. After an initial accumulation phase, excess pore water pressures started to decrease, the earthquake still running.

The triggering of excess pore pressure dissipation during the seismic excitation indicates a partially-drained phenomenon occurring in the model, i.e. on one hand, the soil dynamically strained generates excess pore pressure, and on the other hand, the established hydraulic gradient triggers upward seepage [83,84].

Generation of excess pore pressure prevailed only in the first few seconds, then dissipation and drainage prevailed at all depths, increasing upward, as also confirmed by the measured accelerations (strain softening associated with the development of excess pore water pressures typically attenuates the propagating seismic waves).

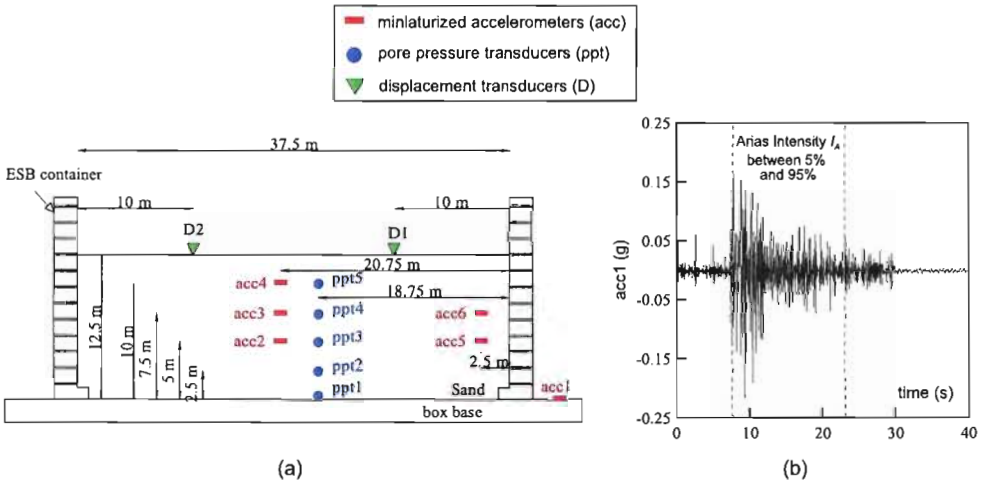


**Fig. 3.** – (a) Schematic view of the model used in the centrifuge test at prototype scale and (b) input seismic accelerogram applied at the base.

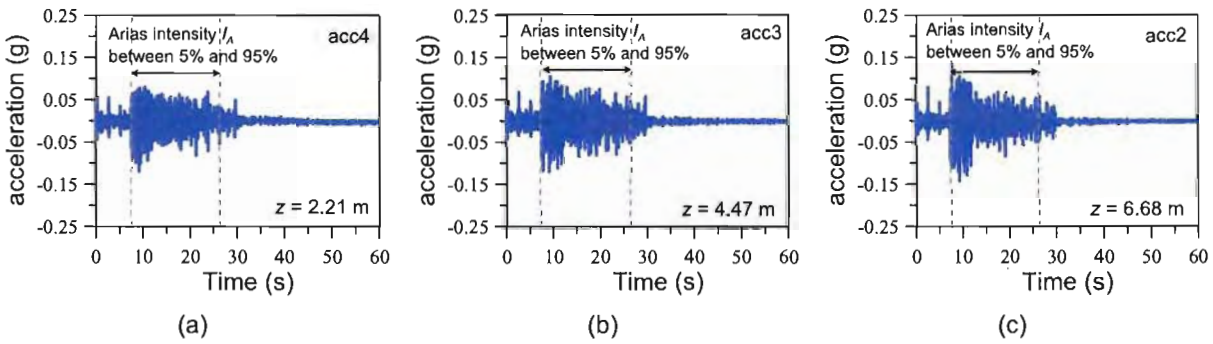


**Fig. 4.** – Accelerograms recorded at various prototype depths in the centrifuge test.

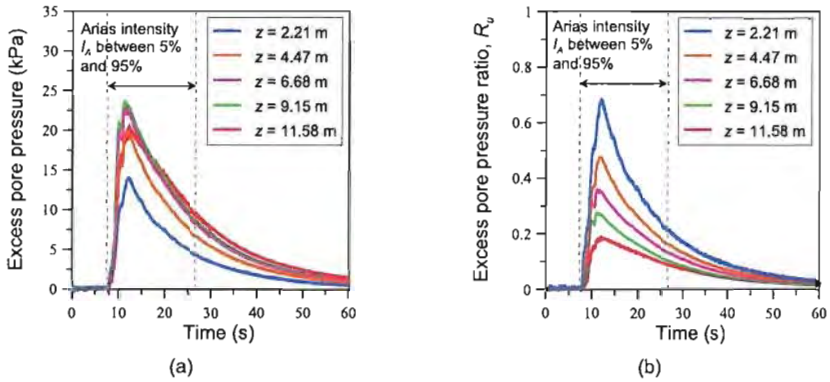


**Fig. 5.** – Excess pore water pressure time histories at various prototype depths observed in the centrifuge test.

### 3.3. Laboratory cyclic simple shear tests for PWP model calibration

Undrained cyclic simple shear tests were conducted at the University Mediterranea of Reggio Calabria on clean Ticino sand specimens using a modified NGI-type simple shear (SS) device [85]. In this SS device, the specimens having a diameter of 80 mm and a height of 20 mm were laterally confined by a wire-reinforced rubber membrane to prevent any lateral deformation (i.e. reproducing $K_0$ conditions). The specimens were prepared in a broad range of relative densities, between 40 % and 90 %, using the moist tamping (MT) reconstitution method. In the present study, the moist tamping technique consisted in placing inside the reinforced membrane two 10 mm high layers of wet sand to achieve the target relative density. Each layer was compacted to a specified height and the effect of vertical inhomogeneity was considered negligible due to the specimen's limited height.

Undrained cyclic SS tests were performed in both stress- and strain-controlled modes. For the stress-controlled cyclic SS tests, they were stopped in correspondence of liquefaction phenomena, i.e. when a single amplitude shear strain ($\gamma_{SA}$) of 3.75 % was attained, in accordance with previous studies [8,86,87]. It was demonstrated that this shear strain level was associated with a quasi-stable value of limiting excess pore water pressure ratio $R_{u,f}$ [8,88]. On the other hand, for the strain-controlled cyclic SS tests, they were conducted up to 15 loading cycles. In all tests, the specimens were consolidated to a predetermined effective vertical stress ($\sigma'_{v0}$) of 100 kPa, after which cyclic shear stress ($\tau_{cyc}$) or cyclic shear strain ($\gamma_{cyc}$) was applied under stress- or strain-controlled conditions, respectively. The applied cyclic stress ratios ($CSR = \tau_{cyc}/\sigma'_{v0}$) ranged from 0.12 to 0.25, while the applied cyclic shear strain ranged from 0.12 % to 0.50 %, and both test types were conducted at a loading frequency of 0.1 Hz. The tests were performed under constant volume conditions to simulate undrained conditions in the NGI simple shear apparatus [89,90]. In constant volume shear tests, the change in vertical stress is assumed to reflect the excess pore pressure that would develop in a true undrained scenario. In particular, an automatic control system maintained constant volume by adjusting the vertical load with vertical strain controlled to less than 0.05 %, in accordance with ASTM D8296 [91]. The experimental program included 19 cyclic simple shear tests, as summarised in Table 2.

#### 3.3.1. Typical experimental cyclic simple shear test results

Fig. 6 presents representative results from stress- and strain-controlled undrained SS tests conducted on two reconstituted specimens of Ticino sand prepared under comparable initial conditions ($D_R$ = 48–54 %, $\sigma'_{v0}$ = 100 kPa). In particular, Fig. 6a, 6c, 6e and 6g deplct typical results from a stress-controlled test subjected to a cyclic shear stress ratio (*CSR*) of 0.16.

In the stress-controlled test, it is apparent that in the first 8 loading cycles the shear strains are not significant, while in the last cycles shear strains increase abruptly attaining liquefaction condition ($\gamma_{SA}$ = 3.75 %) (Fig. 6c). On the other hand, in the strain-controlled test (Fig. 6b, 6d, 6f and 6h), where a constant cyclic shear strain equal to 0.5 % was applied, a progressive reduction of $\tau_{cyc}$ was apparent (Fig. 6b and 6d) and, after about 7 cycles, a limiting condition corresponding to $\Delta u \approx \sigma'_{v0}$ was reached (Fig. 6b and 6h). It is interesting noting that as $N$ increases, the trend and the shape of $W$ and $\Delta u$ differ in stress vs. strain controlled tests. These differences can be ascribed to the specific mode by which the cyclic load is imposed on the soil [92]. In particular, in the strain-controlled test a monotonic increase of $W$ with increasing number of cycles was observed (Fig. 6f), whereas in the stress-controlled test firstly low $W$ values were measured but subsequently an abrupt $W$ rise occurred just in the last loading cycles (Fig. 6e). The different trend of $\Delta u$ (Fig. 6g and 6h) reflects accordingly the different response in terms of $W$.

**Table 2**
– Undrained cyclic simple shear test programme ($\sigma'_{v0}$ = 100 kPa).

| Loading mode | $D_R$ (%) | *CSR* | $\gamma_{cyc}$ (%) |
|---|---|---|---|
| Stress-controlled | 86 | 0.20 | – |
| Stress-controlled | 86 | 0.23 | – |
| Stress-controlled | 86 | 0.25 | – |
| Stress-controlled | 71 | 0.14 | – |
| Stress-controlled | 71 | 0.16 | – |
| Stress-controlled | 71 | 0.18 | – |
| Stress-controlled | 71 | 0.20 | – |
| Stress-controlled | 71 | 0.23 | – |
| Stress-controlled | 54 | 0.12 | – |
| Stress-controlled | 54 | 0.14 | – |
| Stress-controlled | 54 | 0.16 | – |
| Stress-controlled | 54 | 0.18 | – |
| Strain-controlled | 48 | – | 0.12 |
| Strain-controlled | 48 | – | 0.27 |
| Strain-controlled | 48 | – | 0.50 |
| Stress-controlled | 43 | 0.12 | – |
| Stress-controlled | 43 | 0.14 | – |
| Stress-controlled | 43 | 0.16 | – |
| Stress-controlled | 43 | 0.20 | – |

Note: $D_R$ = relative density, *CSR* = applied cyclic stress ratio, $\gamma_{cyc}$ = applied cyclic shear strain.

#### 3.3.2. Calibration of the excess pore-water pressure models by laboratory cyclic simple shear tests

Numerous methodologies have been proposed in the literature to predict the generation of cyclic excess pore water pressure in saturated sandy soils, as thoroughly described in section 2. In the present paper, energy-based and strain-based approaches were considered to assess the performance of these two models using both stress- and strain-controlled CSS test results for comparison purposes. Conversely, the damage-based approach (also categorised as a stress-based approach) was not analysed

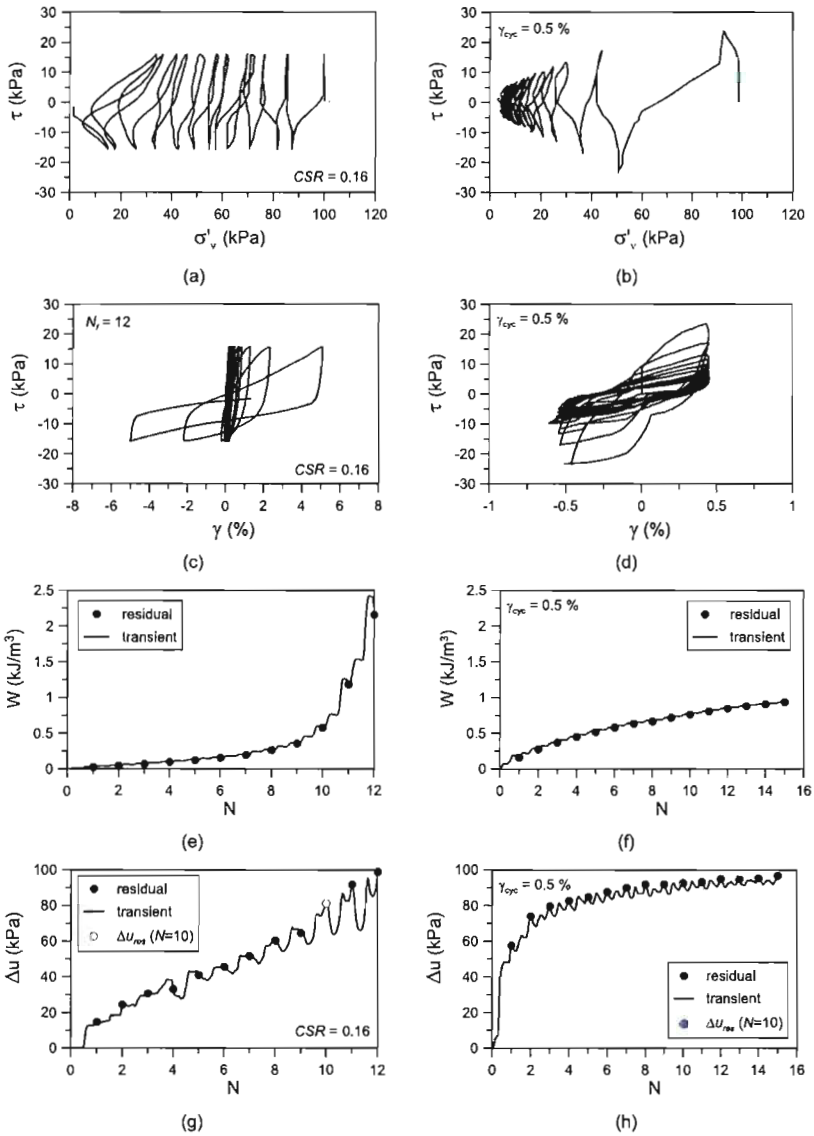


**Fig. 6.** – Typical behaviour of Ticino clean sand ($D_R$ = 51 % ± 3 %; $\sigma'_{v0}$ = 100 kPa) determined in stress-controlled tests (a,c,e,g) and strain-controlled tests (b,d,f,h).

in the present study because only the PWP models accounting directly for cyclic shear strains were considered.

*3.3.2.1. Energy-based PWP model.* To calibrate the energy-based models for Ticino sand using experimental data from undrained CSS tests, the fundamental factors affecting the relationship between residual $R_U$ ($R_{u,res}$) and normalised $W$ ($W_n$) were initially analysed and discussed. Key factors include relative density ($D_R$), applied cyclic stress ratio ($CSR$), and loading mode. The residual values of $R_u$ and $W$ represent the parameters measured at the end of each applied loading cycle, as illustrated in Fig. 6e–6h (indicated by filled circles).

Fig. 7a illustrates the effect of $CSR$ on $R_{u,res}$ versus $W_n$ relationship for Ticino sand tested at the same initial state ($D_R$ = 86 %, $\sigma'_{v0}$ = 100 kPa). It is evident that $CSR$ has a negligible influence on the pattern of pore water pressure generation, consistently with the findings gathered from previous literature studies based on stress-controlled cyclic tests [31,75,93]. The slight dependence of $R_{u,res}$ vs. $W_n$ relationship on $CSR$ as well as loading shape, i.e. irregular, sinusoidal, square or triangular loads, is one of the advantages of the energy-based approach [75,92,94].

Fig. 7b intends to highlight the influence of relative density ($D_R$) on $R_{u,res}$ versus $W_n$ relationship resulting from CSS stress-controlled tests conducted on Ticino sand prepared under various $D_R$ values and subjected to different $CSR$. All specimens were consolidated at the same initial vertical effective stress equal to 100 kPa. In particular, when $D_R$ increases, $R_{u,res}$ was generated more slowly with higher values of normalised cumulative dissipated energy needed to reach failure condition ($W_{n,f}$). Additionally, it is noteworthy that the limiting $R_u$ value ($R_{u,f}$) decreases as relative density increases. Such evidence was found also by other authors in the literature, such as Tomasello and Porcino [28], Yang and Pan [74] and Qin et al. [95]. The experimental evidence that dense materials exhibit a more dilatant behaviour and show less liquefaction tendency is in accordance with critical state theory [96].

On the other hand, the effect of loading mode on the development of the $R_{u,res}$ versus $W_n$ relationship remains poorly understood. Recently, Polito and Martin [92] have demonstrated that the energy-based approach yields to similar $R_{u,res}$-$W_n/W_{n,f}$ relations for undrained stress- and strain-controlled cyclic triaxial tests. In the present study, this

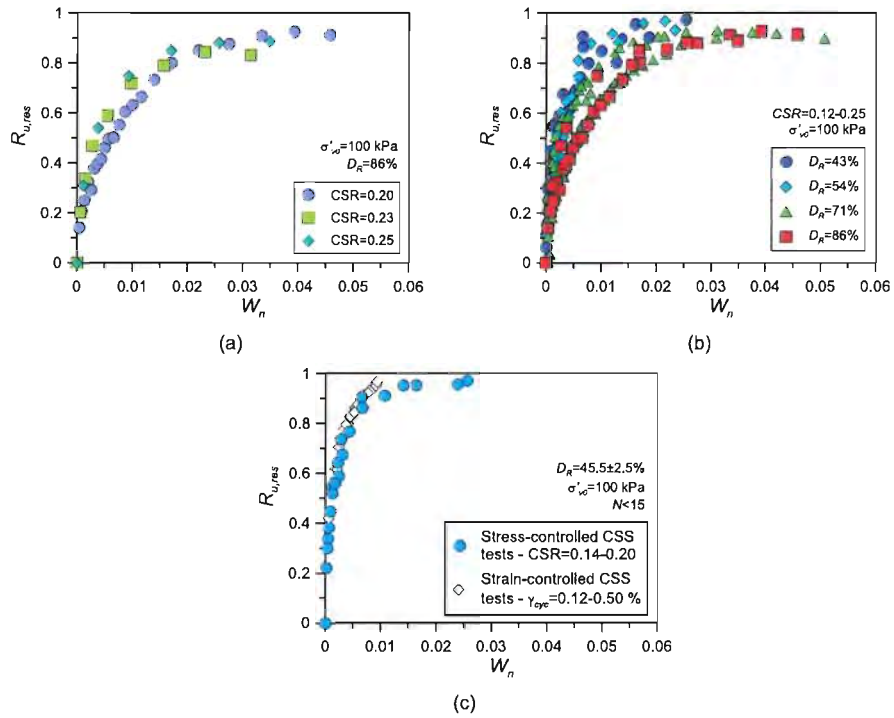


**Fig. 7.** – Relationships between residual excess pore water pressure ($R_{u,res}$) and normalised cumulative dissipated energy per unit volume ($W_n$) from undrained CSS tests carried out on Ticino sand: (a) effect of cyclic stress ratio; (b) effect of relative density; (c) effect of loading mode.

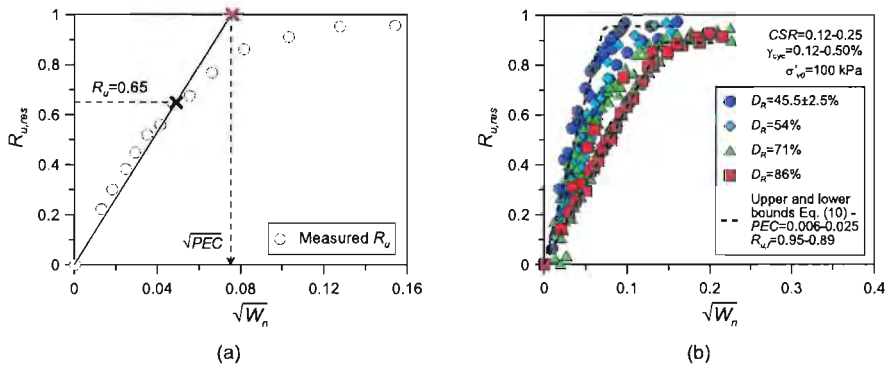


**Fig. 8.** – (a) Graphic procedure adopted to determine *PEC* of the Green et al. [14] model for Ticino sand from undrained stress-controlled CSS data ($D_R$ = 43 %, *CSR* = 0.14), (b) observed bounds of residual $R_u$ vs. $W_n$ curves from CSS tests with different $D_R$.

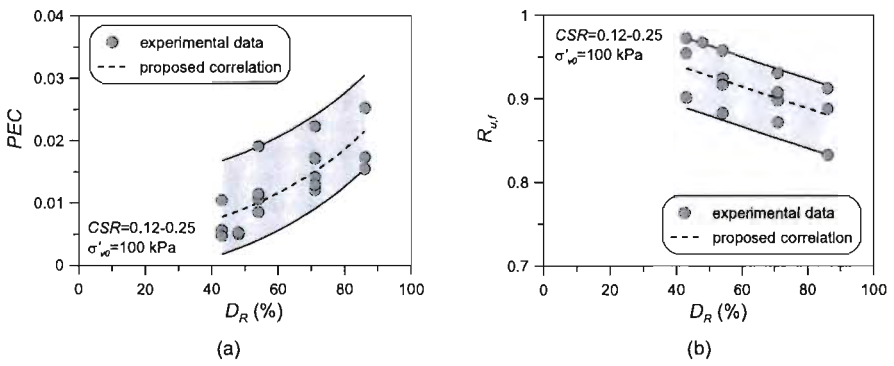


**Fig. 9.** – Trend with $D_R$ of *PEC* and $R_{u,f}$ of the modified GMP model for Ticino sand from undrained CSS tests.

finding remains valid for undrained cyclic simple shear tests (Fig. 7c), which replicate accurately in situ stress conditions before and during an earthquake.

In the original formulation of Green et al. [14] model, a single empirical constant, the *PEC* parameter, is required. This parameter is derived from CSS test data by plotting $R_{u,res}$ against the square root of $W_n$. Specifically, *PEC* is defined as that value on the horizontal axis corresponding to the intersection of two lines, the first one passing through the origin and the point at $R_{u,res} = 0.65$, the second one being the horizontal line at $R_{u,res} = 1$ (Fig. 8a).

The energy-based PWP model originally proposed by Green et al. [14] was revised to incorporate experimental evidence discussed above to enable a more accurate prediction of $R_u$ in the numerical analyses of seismic centrifuge tests conducted on Ticino sand. In addition to *PEC*, the GMP model was further adjusted in the present study to account that $R_{u,f}$ values could be less than unity in dense Ticino sand, as follows:

$$R_u = \sqrt{W_n/PEC} \leq R_{u,f} \tag{10}$$

The performance of the revised model is shown in Fig. 8b on the $R_{u,res}$–$W_n$ plane. Notably, when applied to the CSS test data, the modified model demonstrates a strong fit ($R^2$>0.89) with data points placed within a zone defined by upper and lower bounds corresponding to the following parameters: *PEC* = 0.006–0.025 and $R_{u,f}$ = 0.95–0.89 (Fig. 8b).

The availability of analytical relationships between the model parameters of Eq. (10) and the influence factors is crucial in non-linear seismic site response analyses. Fig. 9 illustrates the variation of *PEC* and $R_{u,f}$ empirical parameters with $D_R$. Some scatter in the experimental data can be observed in Fig. 9, probably due to the variation of *CSR*; for this reason, upper and lower bounds were identified for the subsequent analysis. It is noteworthy that the model parameter *PEC* increases with $D_R$ of the sand, whereas $R_{u,f}$ decreases as $D_R$ increases. The correlations presented in Fig. 9 were employed in the numerical modelling of the centrifuge test.

*3.3.2.2. Strain-based PWP model.* The CSS test results were also analysed to determine the empirical constants of the widely recognised PWP model proposed by Vucetic and Dobry [11] implemented in the software used to perform numerical analyses. Fig. 10 presents the experimental data collected in this study from both stress- and strain-controlled CSS tests conducted on Ticino sand reported in $R_{u,res}$-$\gamma_{max}$ plane considering the same number of loading cycles $N$ = 10. Specifically, in strain-controlled tests, the $R_{u,res}$ values are determined at the end of 10 cycles of applied cyclic shear strain ($\gamma_{cyc}$) (Fig. 6g). In contrast, in stress-controlled tests, the $R_{u,res}$ values correspond to the first occurrence of the recorded maximum strain levels at the 10th loading cycle (Fig. 6h). Fig. 10 also displays the boundary curves proposed by Dobry [97] for clean sands from strain-controlled cyclic triaxial tests for the sake of comparison. The dashed lines in the same figure represent the best-fit curves for the experimental data obtained through regression analysis using the strain-based model proposed by Vucetic and Dobry [11] [Eq. (6)]. In the present study, data points derived from strain-controlled CSS tests on Ticino sand fall inside the range proposed by Dobry [97], whereas the results from stress-controlled CSS tests align with Dobry's lower boundary, in agreement with other authors (Cetin and Bilge [12], among others). Notably, the data from the stress-controlled tests fall to the right of their strain-controlled counterparts resulting in lower $R_{u,res}$ values. Such differences could be explained considering the different stress path between stress- and strain-controlled tests. Therefore, this difference makes a direct comparison between the two types of tests potentially misleading [12]. Additionally, the relationship between $R_{u,res}$ and $\gamma_{max}$ for both loading modes appears poorly dependent on sand's relative density (Fig. 10).

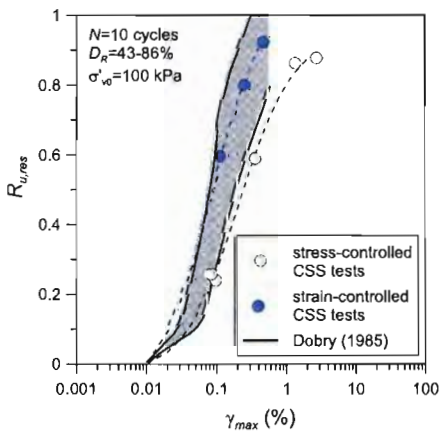


**Fig. 10.** – Trend of residual $R_u$ with maximum shear strain obtained in the present study by stress- and strain-controlled undrained CSS tests on Ticino sand and comparison with the upper and lower bound curves proposed by Dobry [97] for clean sands.

The regression analysis conducted using Eq. (6) yields the parameters *p*, *f*, *F*, and *s* listed in Table 3. Despite the limited number of strain-controlled CSS tests, Table 3 would highlight that *p*, *f*, and *s* are similar for strain- and stress-controlled tests, whereas *F* accounts for the differences observed in Fig. 10.

## 4. Numerical simulations of the seismic centrifuge test

To simulate the response observed in the centrifuge test (prototype scale) described in section 3.2, non-linear effective site response analyses were conducted using DEEPSOIL v.7.1.2 [53]. The bottom boundary was assumed fixed and impermeable, so that dissipation was only allowed to occur at the surface. The water table was placed at the top of the Ticino sand column, as illustrated in Fig. 11. Recording acc1 was used as input motion and the excess pore water pressures were allowed to build-up and dissipate as well. The dissipation model was based on Terzaghi 1-D [98] consolidation theory, where the consolidation coefficient $C_v$ is a key parameter required for the analysis. The coefficient $C_v$, which can be expressed as a function of permeability coefficient $k$ and constrained modulus $M$, $C_v$=$(k \cdot M)/\gamma_w$, is assumed to be variable with depth in the numerical model (Fig. 11f).

### 4.1. Input parameters

Fig. 11 shows the profile of the input soil parameters required for the numerical analyses. As for input parameters relative to PWP generation models [Eqs. (6) and (10)], they were previously discussed in section 3.3.2. Nevertheless, one aspect to be underlined is that $W_n$ (dimensionless) has to be expressed in percentage to meet the requirements of the DEEPSOIL code. Furthermore, preliminary sensitivity numerical analyses suggested to set *PEC* values variable with depth, i.e. the upper values of the band (Fig. 9a) were assigned at the base of the centrifuge model, whereas the lower values (Fig. 9a) were assigned at the top of the centrifuge model. A possible explanation of this variation with depth can be found considering the influence of other factors, different from $D_R$, which could affect *PEC* values (e.g. *CSR*, $\sigma'_{v0}$, among others). In addition,

**Table 3**
Empirical parameters of Vucetic and Dobry [11] model for Ticino sand reported in Fig. 10.

| Loading mode | *p* | *f* | *F* | *s* | $R^2$ |
|---|---|---|---|---|---|
| Stress-controlled | 0.951 | 1 | 0.538 | 1.083 | 0.99 |
| Strain-controlled | 1.098 | 1 | 1.193 | 1.059 | 0.99 |

Note: *p*, *f*, *F*, *s*= parameters of VD model [Eq. (6)]; $R^2$ = coefficient of determination.

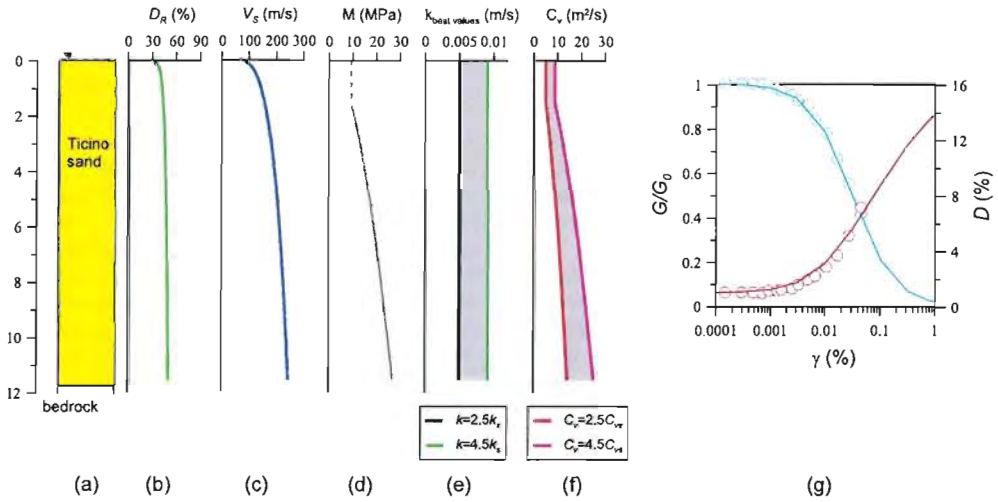


**Fig. 11.** – Profiles of the soil parameters used in the numerical analyses of centrifuge test: (a) soil profile at prototype scale, (b) relative density, (c) shear wave velocity, (d) constrained modulus, (e) permeability coefficient, (f) consolidation coefficient; and (g) normalised shear modulus and damping ratio versus shear strain for Ticino sand.

the adopted variation of *PEC* parameter with depth is supported by previous studies [52,80], which reported an underestimation of excess pore water pressure at shallow depths when an energy-based model was applied.

- $D_R$ profile

Traditional methods for determining the relative density in centrifuge tests rely on measurements of the model mass and volume even if alternative methods have also been proposed in the literature [99]. In the present study, the relative density determined by global measurements of mass and volume resulted 47 %. Nevertheless, $D_R$ value based on mass-volume measurements can be affected by errors [43]; for this reason, experience gained at ISMGEO indicated that soil relative density can be better deduced by back-analysis of measured inflight settlements. This method follows a trial-and-error approach, in which the model is divided in $j$ sub-layers, whose unit weight and void ratio are adjusted iteratively. In particular, for each $j$th sub-layer the current values of unit weight and void ratio are computed as follows:

$$\gamma_{d,j,l} = (G_s \cdot \gamma_w) / (1 + e_{j,l}) \tag{11a}$$

$$\sigma'_{v,j,l} = \gamma_{d,j,l} \cdot t_p + \sigma'_{v,j-1,l} \tag{11b}$$

$$e_{j,l+1} = e_{j,l} - C_c \cdot \log\left(\sigma'_{v,j,l}\right) \tag{11c}$$

where:

$t_p$ and $\gamma_{d,j,l}$ are the thickness and dry unit weight of the $j$th–layer at the $l$th–iteration. The process utilises the average compression index ($C_c$), estimated from the total surface settlement of the soil model (i.e. 56.47 mm), to calculate the density profile. The iteration procedure is usually concluded after 3 to 5 iterations $l$ when the convergence error is $|e_{j,l+1} - e_{j,l}| < 10^{-8}$. The resulting profile indicates the sample density to vary between 28 % (at the sample surface) and 48.5 % up to a depth of 11.5 m.

- $V_S$ profile

Shear wave velocity ($V_S$) profile (and related initial shear modulus $G_0$) was gathered from bender element tests in triaxial apparatus [100] performed on pluvial deposited Ticino sand specimens prepared at different values of relative density.

The following equation was found:

$$V_S = C_S \cdot \left[f(e) \cdot (p'/P_a)^{2m}\right]^{0.5} \tag{12}$$

where $C_S$ = experimentally determined material constant = 235, $f(e)$ = generalised void ratio function = $e^{2d} = e^{-0.8}$, $p'$ = mean effective stress and $P_a$ is the atmospheric pressure (i.e. 100 kPa), and $m$ coefficient = 0.22.

$V_S$ values for Ticino sand in centrifuge test were determined basing on Eq. (12) considering $D_R$ and $p'$ values of the model. In particular, the void ratio $e$ ranged from 0.82 to 0.75 with a target value equal to 0.76 ($D_R$ = 47 %). For $p'$ calculations, the effective horizontal stress was assumed as $\sigma'_{h0} = [1\text{-}\sin(\varphi')] \cdot \sigma'_{v0}$, being $\varphi' = \varphi'_{cs}$ the internal friction angle at critical state (Table 1).

- $M$ profile

The constrained modulus ($M$) profile was gathered by oedometer tests carried out on Ticino sand and the relationship between $M$ and stress level (i.e. depth) resulted [Eq. (13)]:

$$M = a \cdot P_a \cdot \left(\frac{\sigma'_{v0}}{P_a}\right)^b \tag{13}$$

where $a$ and $b$ are emplrical constants specifically calibrated through the aforementioned oedometer tests with values equal to 255 and 0.54, respectively.

- $k$ profile

The importance of selecting proper values of permeability coefficient $k$ in effective stress seismic analysis is reported by several authors [44, 46–50,101]. In fact, $k$ values affect both build-up and dissipation of excess pore water pressures; furthermore, $k$ can be different from the initial static value ($k_s = 2 \cdot 10^{-3}$ m/s) and can also vary during the earthquake. Several relationships between (variable) permeability coefficient and excess pore water pressure ratio in all build-up, liquefaction and dissipation phases were proposed in the literature [49–51,101]. In the present study, average values of $k$ (constant with depth) in the range from $2.5 \cdot k_s$ to $4.5 \cdot k_s$ were assumed. This range resulted from the relationships $k/k_s = f(R_u)$ calibrated by centrifuge model tests proposed

by Shahir et al. [49] in build-up phase ($R_u < 1.0$) which represents the case of the centrifuge test in the present study. In particular, for the depths between 2 m and 10 m, $k/k_s$ permeability ratio (average values calculated for the duration of earthquake at a given depth) were in the range 2.5–4.5. These values are also consistent with the experimental findings gathered by the authors from previous research [51].

- Normalised modulus reduction $G/G_0$ curve and damping factor $D$

The normalised modulus reduction $G/G_0$ curve and damping factor $D$ curve used in the numerical analyses were gathered from resonant column tests performed on Ticino sand. Stress-strain curve was interpreted by the non-linear constitutive model implemented in DEEPSOIL [53], namely modified hyperbolic model Matasović and Vucetic [102] termed as the MKZ (modified Kondner and Zelasko [103] model); a non-Masing rule, termed as the modulus reduction and damping factor (MRDF), was employed. For the degradation indices of shear modulus ($\delta_G$) and shear strength ($\delta_\tau$), the curve fitting parameter $\nu$ termed as the degradation parameter resulted 2.91, in accordance with the range from 1 to 5 reported for cohesionless soils in previous literature studies [52,104,105].

The stress-strain relationship of the implemented MKZ model is the following:

$$\tau = \frac{\gamma \cdot G_0 \cdot \delta_G}{1 + \beta^* \cdot \left[\frac{\gamma}{(\tau_{max} \cdot \delta_\tau)/(G_0 \cdot \delta_G)}\right]^{s^*}} \tag{14}$$

where $\tau$ is the shear stress, $\gamma$ is the shear strain, $\beta^*$ and $s^*$ are curve fitting parameters. The degradation indices reported in Eq. (14) adjust the unloading-reloading equation during excess pore water generation to incorporate the mobilised shear stress reduction as follows [Eq. (15)] [61]:

$$\delta_G = \sqrt{1 - R_u} \tag{15a}$$

$$\delta_\tau = 1 - R_u^\nu \tag{15b}$$

### 4.2. Results

The measured and computed time-histories of residual excess pore

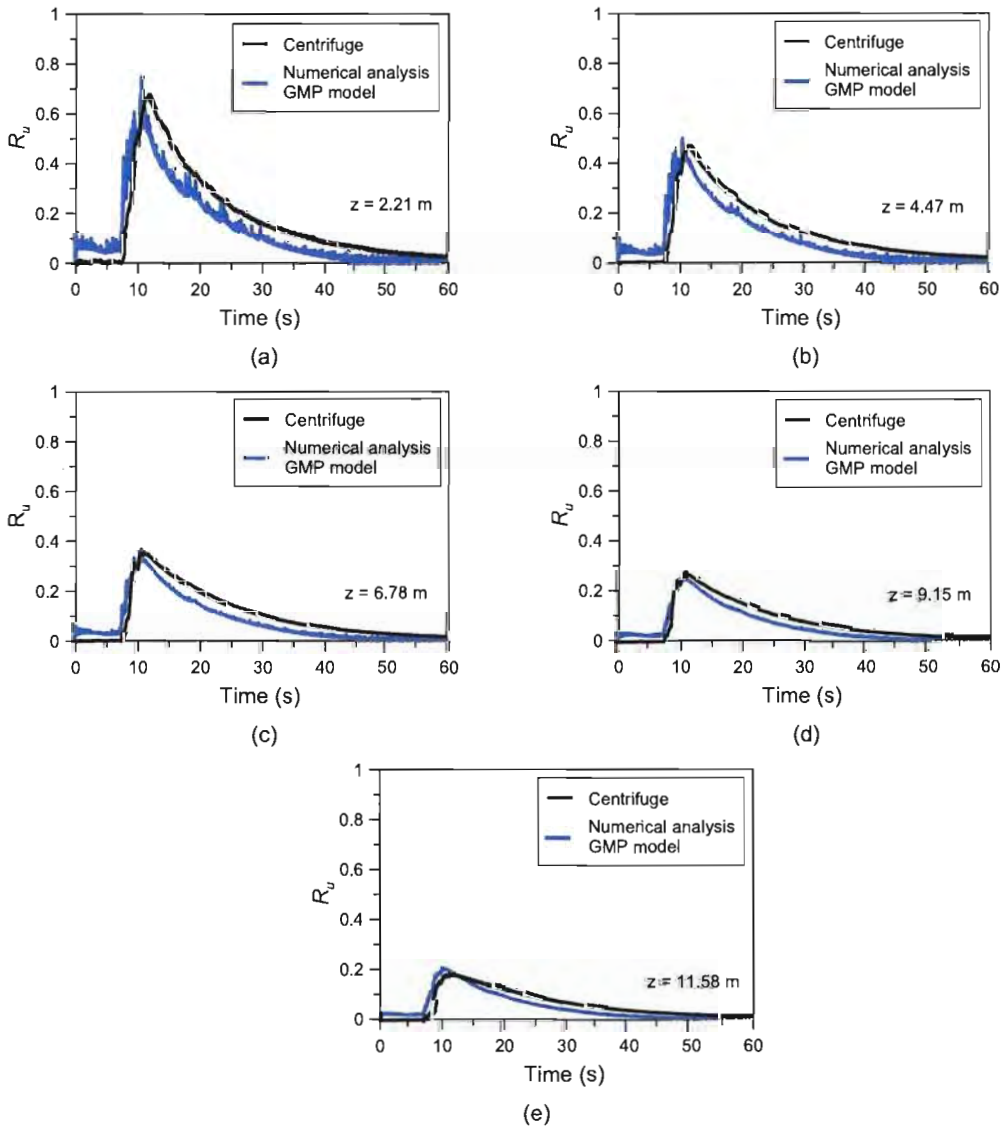


Fig. 12. – Comparison between measured and predicted trends of residual $R_u$ with time at various depths using GMP model ($k = 2.5 \cdot k_s$).

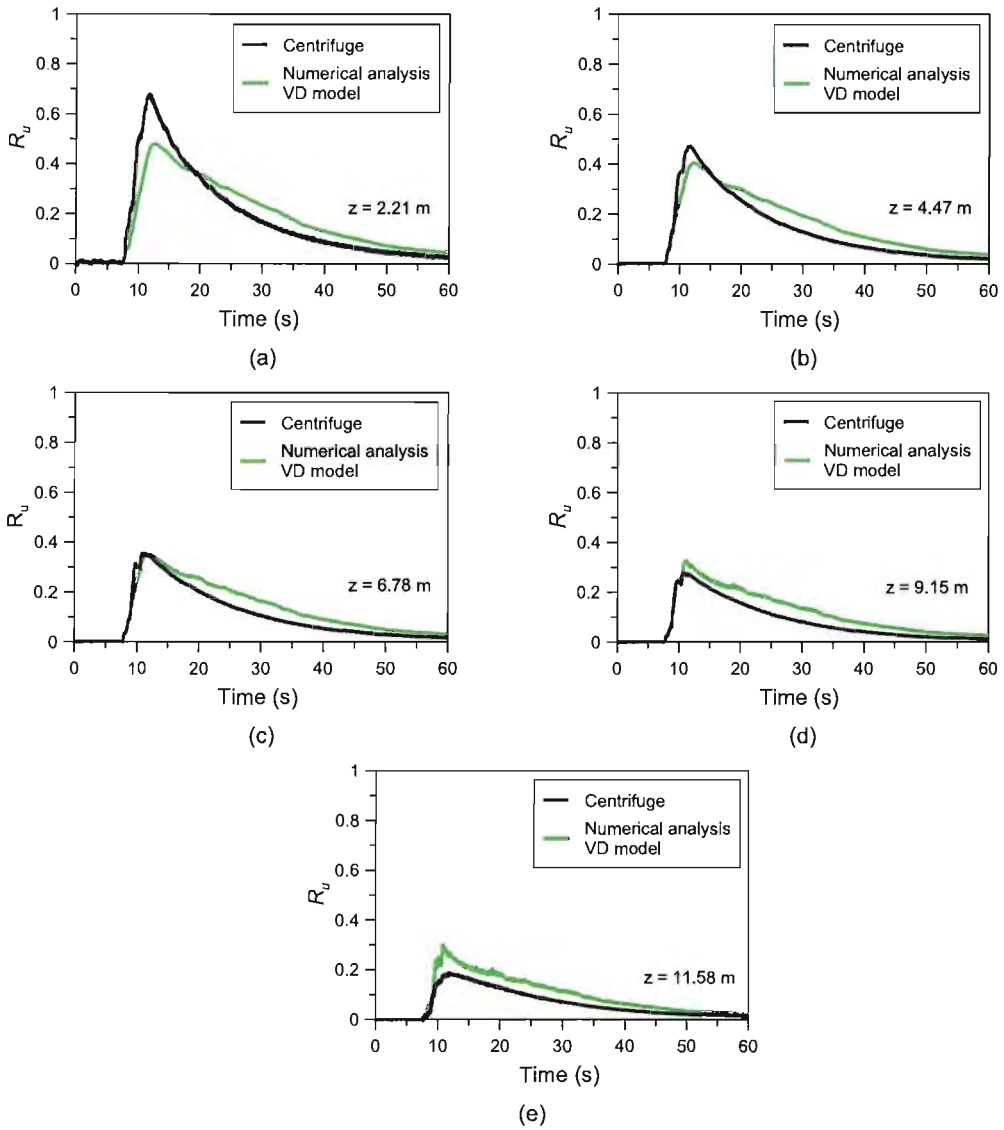


**Fig. 13.** – Comparison between measured and predicted trends of residual $R_u$ with time at various depths using VD model ($k = 4.5{\cdot}k_s$).

pressures and accelerations using the PWP models are presented in Figs. 12 and 13. In particular, for different depths corresponding to ppt1, ppt2, ppt3, ppt4 and ppt5, Fig. 12 reports $R_u$ vs. time gathered from numerical analysis using GMP model and, for comparison purposes, the corresponding trends measured in the centrifuge model test. A favourable overall agreement between measured vs. computed PWP trends can be observed at different depths. Consistently with experimental measurements, $R_u$ values are well below unity value even at low depths. In the first phase of the input motion up to 7 s, it is evident that non zero values of $R_u$ are computed by numerical analysis, whereas in the centrifuge test there is practically no build-up of excess pore water pressures. This discrepancy can be explained considering that in energy-based models, the dissipated energy is calculated even if shear strains are less than a threshold value, as it happens in the centrifuge due to the background noise produced by the rotation. For this reason, the energy-based approach provides $R_u \neq 0$ even for very low values of $W$. An improvement could be obtained by the introduction of a limiting shear strain level below which no dissipated energy is calculated and consequently $R_u$ values would result equal to zero. The numerical results obtained considering as input parameter $k = 2.5{\cdot}k_s$ for Ticino sand illustrate that a satisfactory agreement is attained in terms of peak $R_u$ and dissipation behaviour between experimental and predicted measurements.

Fig. 13 shows both pore water pressure response from 1D analysis using VD model, calibrated through strain-controlled CSS tests, and centrifuge measured values. Using the VD model, an underestimation between computed and measured $R_{u,max}$ at low depths, i.e. 2.21 m and 4.47 m, was obtained with differences of 30 % and 14 %, respectively. Conversely, a reasonable correspondence was observed for all the other cases. This discrepancy at depths near the surface was also observed by other authors based on 1D effective stress site response analyses [52] even fully coupled [106,107]. A value of inflight permeability $k = 4.5{\cdot}k_s$ was found to match better the dissipation response at all depths, as shown in Fig. 13.

To compare the response of recorded and computed accelerations at different depths, 5 % damped acceleration response spectra of the acceleration time-histories using the two PWP models are displayed in Fig. 14. The recorded acceleration time-histories refer to acc4, acc3 and acc2, corresponding to 2.21 m, 4.47 m and 6.68 m, respectively.

At medium depths (z = 6.68m), calculated accelerations using both

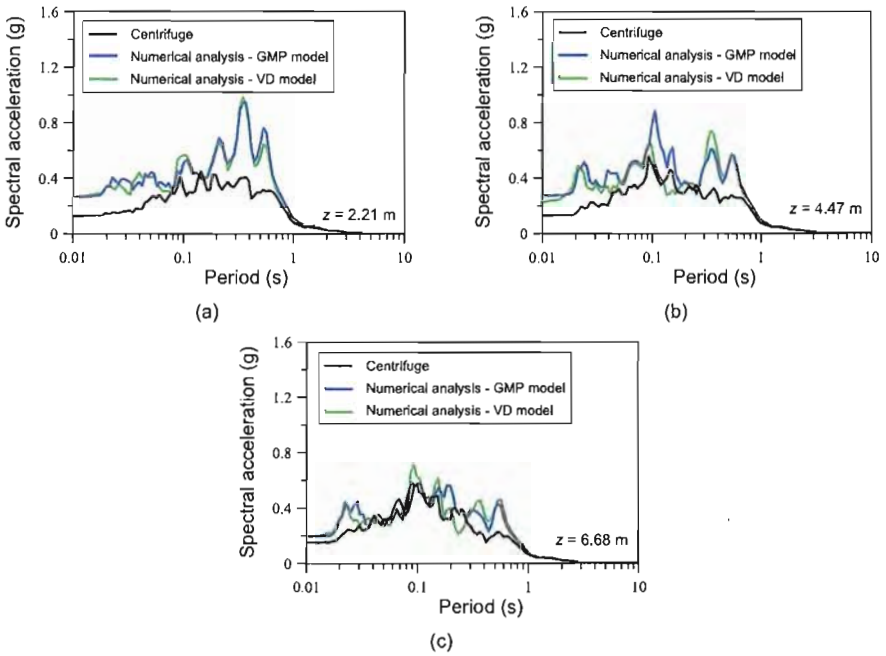


**Fig. 14.** – Comparison between measured and the predicted 5 % damped acceleration response using GMP and VD models at various depths.

PWP models are agreeable with respect to measured ones; nevertheless, near the surface ($z$ = 2.21 m), the simulated response spectra are significantly higher (overprediction) compared with the recordings as well as Arias Intensities. In particular, the presence of some acceleration spikes at certain frequencies is apparent in the predicted trends. These discrepancies between the measured and calculated spectra accelerations values especially at low depths were observed also by other authors in 1D seismic response analysis vs. centrifuge measurements, such as Pervaiz et al. [52] and Ramirez et al. [106].

To provide an overall interpretation of numerical simulations against experimental measurements in centrifuge, Fig. 15 presents the profiles of $R_{u,max}$, PGA, and maximum shear strain ($\gamma_{max}$) with depth. The experimental $\gamma_{max}$ values were derived from acceleration measurements in the centrifuge, following the procedure proposed by Zeghal and Elgamal [108].

The analysis of Fig. 15 indicates:

- a satisfactory agreement in terms of $R_{u,max}$ between experimental and predicted values by using GMP model, whereas when VD model is adopted an underestimation was observed at shallow depth;
- an apparent overprediction of PGA values, regardless of PWP model;

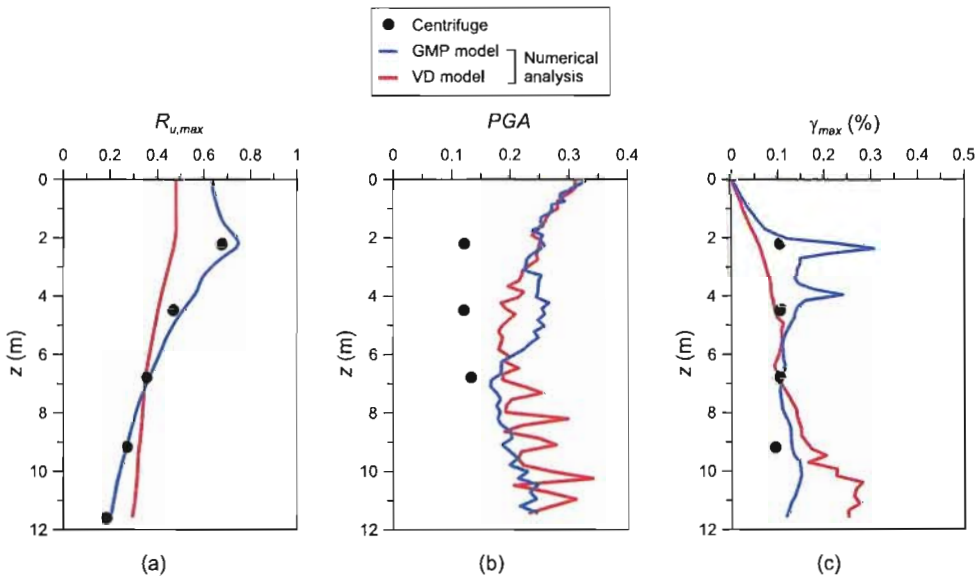


**Fig. 15.** Comparison between measured and predicted $R_{u,max}$ (a), *PGA* (b) and $\gamma_{max}$ profiles using GMP and VD models.

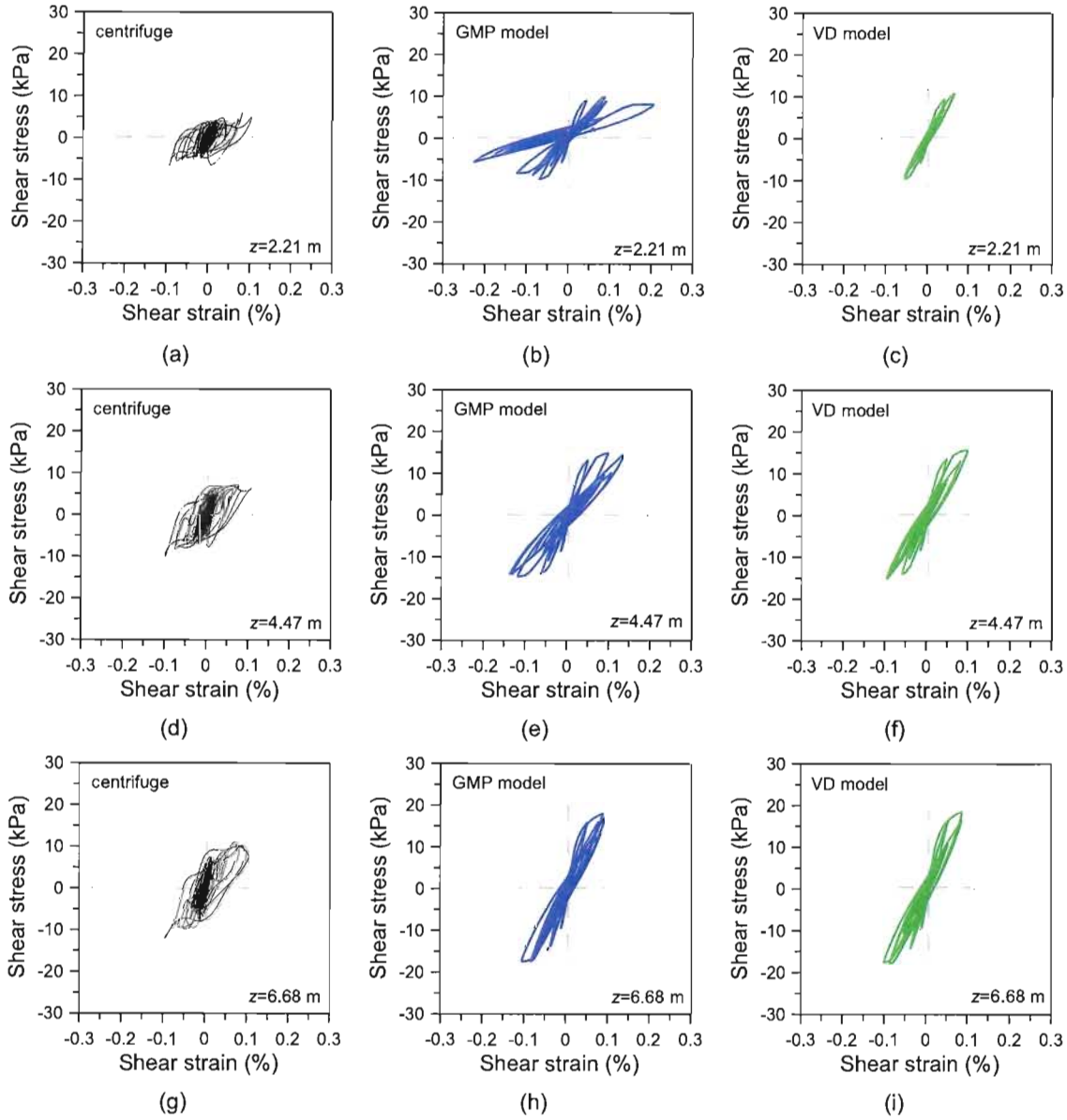


**Fig. 16.** – Comparison between measured and predicted stress-strain loops using GMP and VD models.

- a reasonable agreement between $\gamma_{max}$ predictions from numerical simulations and experimental data.

Fig. 16 shows the stress-strain loops at different depths gathered by numerical analysis together with those obtained indirectly through the aforementioned procedure proposed by Zeghal and Elgamal [105]. Although some discrepancies can be observed in numerical vs. experimental results, Fig. 16 demonstrates a relatively reasonable agreement. Notably, it is interesting to observe that the numerical analysis carried out using the GMP model appears to better capture the stiffness degradation observed in the centrifuge tests compared to the results obtained with the VD model, suggesting a more accurate representation of the soil's nonlinear response under cyclic loading conditions. The differences observed in shear stress values were expected to occur due to the acceleration overestimation, especially at shallow depths (Fig. 15b).

Finally, a possible explanation of the observed discrepancies in terms of acceleration profiles (Fig. 15b) and shear stress-strain loops (Fig. 16) could be attributed to the fact that the modified hyperbolic Kondner and Zelasko model is inherently unable to capture the dilative behaviour of soil, which is expected at shallow depths. Furthermore, such non linear model does not account for density changes associated with PWP build-up and the corresponding updates of input parameters [52].

These results highlight that if a given PWP model is able to capture the response in terms of $R_u$ in a satisfactory way, it does not mean that at the same time it predicts well the response in terms of accelerations. The finding that can be drawn by the present study and other previous

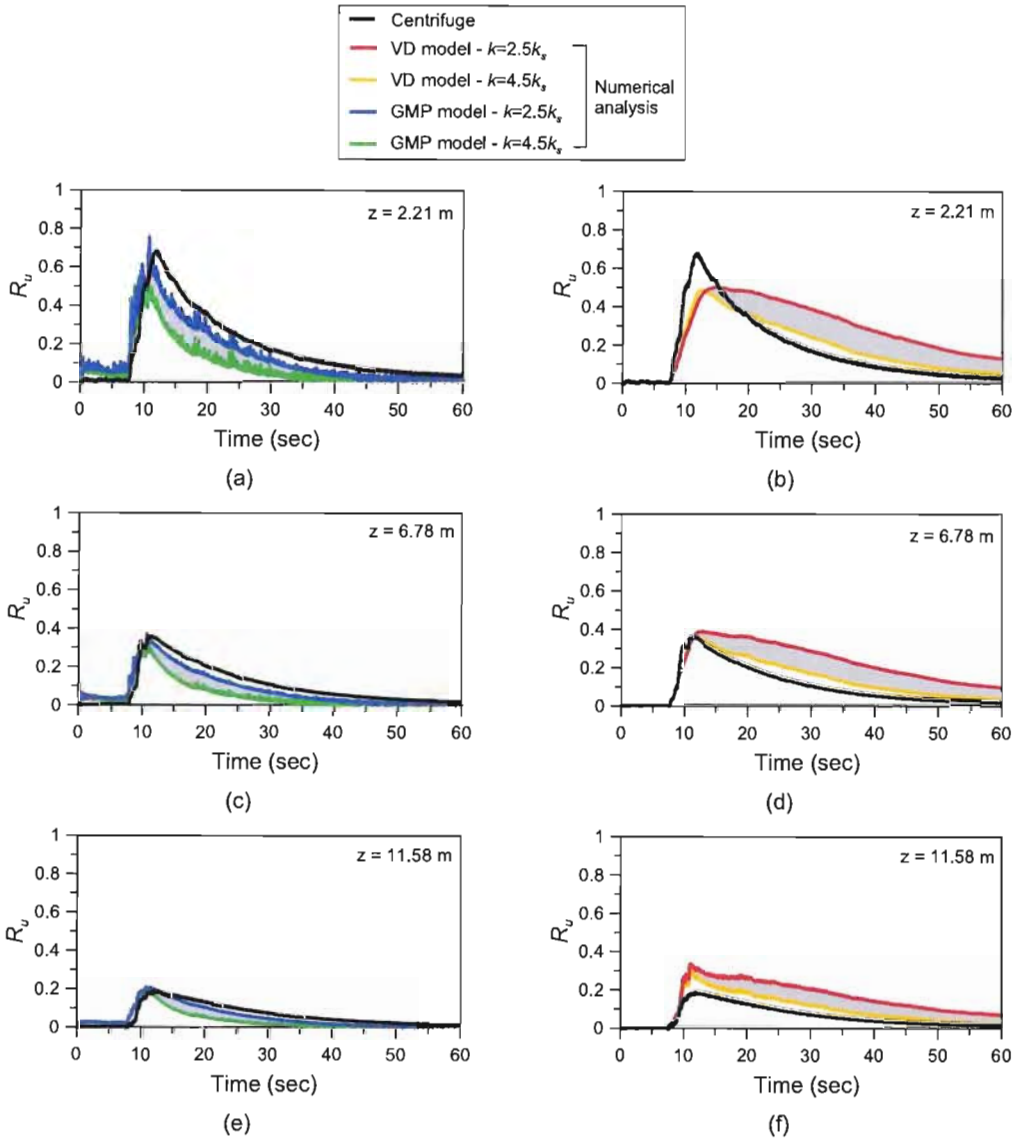


Fig. 17. – Comparison between measured and predicted trend of residual $R_u$ with time at various depths using: (a,c,e) GMP model, (b,d,f) VD model.

research [52,106,107] is that, in general, at depths far from the surface one can expect a more reasonable agreement between computed and measured accelerations. This aspect would require further research to explore all input factors ($V_s$, $k$, $\sigma'_{v0}$, etc) affecting the acceleration response when a given pore water pressure generation model is used in the numerical analysis.

### 4.3. Discussion

The selection of an appropriate value of $k$ and consequently of $C_v$ in 1D non-linear seismic response analysis appears crucial, especially when the seismic loading causes the triggering of liquefaction [46,49,51]. To verify the influence of permeability coefficient (assumed constant with depth) on the calculated pore water pressure response, the simulations were repeated using the lower and the upper values of the $k$ range (2.5–4.5·$k_s$). Fig. 17 reports for the two analysed PWP generation models, i.e. GMP and VD models, the variation of generated and dissipated pore pressure with time at different depths.

For GMP model (Fig. 17a, 17c and 17e), a value of $k = 2.5 \cdot k_s$ improves the accuracy of the numerical results at all depths in terms of maximum excess pore water pressure and dissipation rate, compared to the corresponding trend gathered when using a higher value of $k$. On the other hand, for the VD model (Fig. 17b, 17d and 17f), a value of $k = 4.5 \cdot k_s$ improves the numerical predictions, especially in terms of dissipation rate, compared to the corresponding trend when using a lower value of $k$, i.e. 2.5·$k_s$. It is worth mentioning that the VD model appears more sensitive to the variation of $k$ especially in the post-peak phase of $R_u$ with respect to the GMP model.

Since previous literature studies (e.g., Dash and Sitharam [109], Mei et al. [62], among others) have calibrated strain-based models using stress-controlled test data, it is valuable to verify the influence of loading mode (i.e. stress-vs strain-controlled undrained CSS tests) on pore water pressure response in numerical simulations. For this reason, Fig. 18 intends to show the time-histories of excess pore water pressure at several depths obtained by numerical simulations together with the experimental measurements for comparison purposes. The results refer to the VD model only since for the GMP model it was verified (Fig. 7c) that the loading mode (stress-vs. strain-controlled tests) has a minor influence on

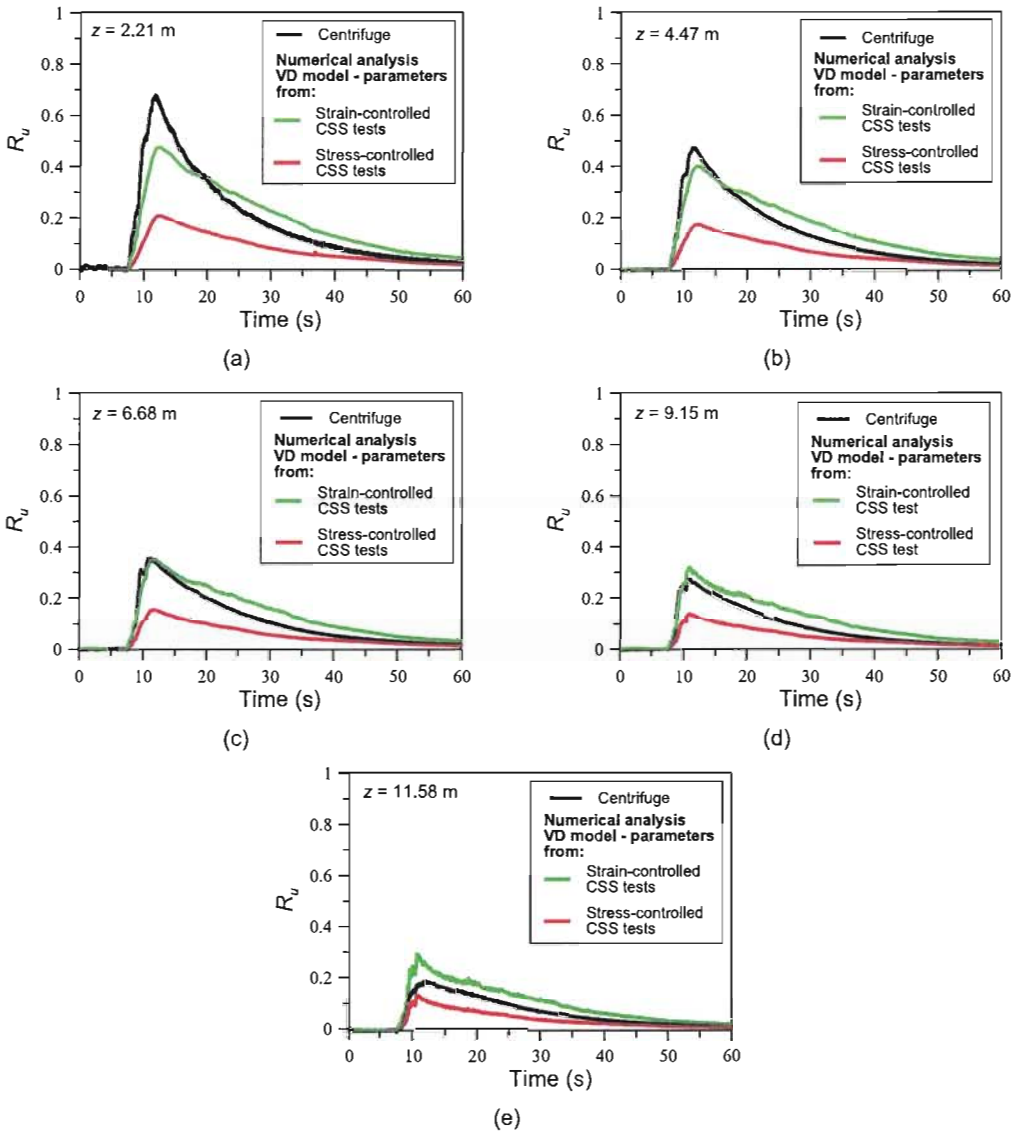


**Fig. 18.** – Comparison between measured trend of residual $R_u$ with time at a given depth and predicted one gathered by numerical analysis using VD model calibrated from strain- and stress-controlled CSS tests ($k = 4.5 \cdot k_s$).

the $R_{u,res}$-$W_n$ relationship and for this reason this aspect was ignored. Fig. 18 illustrates that, when laboratory undrained stress-controlled SS tests are used to calibrate the VD PWP model (Table 3), a significant underestimation of pore water pressure build-up is apparent with differences in percent that are equal to 55 % at all depths.

Finally, to obtain reliable results from numerical analysis, it appears important to derive the empirical parameters of the PWP models taking into account the influence of key factors, such as loading mode and stress path (triaxial, simple shear, torsional). In particular, for strain-based model, it is recommended using calibration parameters from strain-controlled undrained cyclic tests to improve the accuracy of PWP numerical predictions.

## 5. Summary and conclusions

The paper presents a comprehensive study focused on the validation of two pore water pressure (PWP) models, specifically the GMP and VD models, through numerical simulations of a selected seismic centrifuge test performed on Ticino sand. The two PWP models which are implemented in the 1-D site response analysis program DEEPSOIL were rigorously calibrated using high-quality undrained cyclic simple shear (CSS) tests conducted on Ticino sand reconstituted at varying initial states ($D_R$ = 40–90 %) and subjected to different *CSR* or $\gamma_{cyc}$ values. These CSS tests replicate in a realistic way in situ ground conditions before and during earthquakes if compared with respect to traditional cyclic triaxial tests. To achieve a more accurate numerical prediction in terms of PWP, the original energy-based GMP model was revised by introducing an additional calibration parameter $R_{u,f}$. In addition, the calibration of soil parameters (e.g., permeability coefficient $k$, constrained modulus $M$, shear wave velocity $V_S$, normalised shear modulus $G/G_0$ and damping $D$ curves) was based on high-quality lab tests specifically performed on the same material used in the centrifuge test. This approach enhances the accuracy and reliability of the results.

The main conclusions of the study are the following.

- The key factors ($D_R$, *CSR*) influencing the development of PWP from laboratory tests were analysed. The results of undrained CSS tests reveal that the parameters *PEC* and $R_{u,f}$ of the GMP model are

significantly influenced by $D_R$, whereas *CSR* has a negligible effect. On the other hand, the empirical parameters of the VD model are found to be barely dependent on both *CSR* and $D_R$. Based on these findings, appropriate correlations to derive the necessary model calibration parameters were developed.

- From the results of stress- vs. strain-controlled CSS tests conducted on Ticino sand it appears that the energy-based relationship $R_{u,res}$-$W_n$ is poorly influenced by the loading mode (Fig. 7c) while this latter strongly influences the resulting relationship $R_{u,res}$-$\gamma_{max}$ of the VD model with lower $R_{u,res}$ values obtained in case of stress-controlled cyclic tests against strain-controlled ones (Fig. 10).
- During the seismic excitation in the centrifuge test, all the peak $R_u$ values, higher at the surface and decreasing downward, occurred almost simultaneously in the first 12 s at all depths (Fig. 5). A maximum $R_u$ value of 0.7 was measured at a depth of 2.2 m indicating that full liquefaction condition was not triggered. After an initial accumulation phase, excess pore water pressures started to decrease, the earthquake still running indicating that a partially-drained phenomenon occurred in the model.
- The comparison between measured (from the centrifuge test) and computed (from the numerical analysis) PWP response illustrates a good agreement at all depths for the GMP model (Fig. 12); conversely, the VD model underestimates $R_{u,max}$ at shallow depths when the calibration of model parameters was made through CSS test in strain-controlled mode (Fig. 13).
- The selection of an appropriate permeability coefficient $k$ is crucial in 1-D non-linear seismic response analyses. In the present study, average values of $k$ (constant with depth) in the range from $2.5 \cdot k_s$ to $4.5 \cdot k_s$ were assumed based on the relationships $k/k_s = f(R_u)$ proposed in the literature and calibrated by centrifuge model tests. In particular, for the GMP model, a value of $k = 2.5$ times the initial static value ($k_s$) improves the numerical accuracy in terms of maximum excess pore water pressure and dissipation rate. In contrast, for the VD model, a value of $k = 4.5 \cdot k_s$ yields improved predictions, particularly for the dissipation rate. Notably, the VD model demonstrates greater sensitivity to variations in $k$ compared with the GMP model, especially in the post-peak phase of $R_u$.
- Calculated spectral accelerations using both PWP models are in good agreement with measured spectral accelerations only at the middle of the box, whereas near the surface ($z \leq 4.47$ m) the simulated response spectra are overpredicted compared to the recorded values (Fig. 14).

Considering the opposing findings gathered from previous research on this topic in the literature, an extensive database and further numerical modelling are needed to reach more definitive conclusions even for dynamic centrifuge tests performed on various soils experiencing full liquefaction condition.

## Funding

This research has been carried out within the framework of the National Recovery and Resilience Plan (PNRR), Mission 4, Component 2, Investment 1.5, funded by the European Union-NextGenerationEU for the realization of Innovation Ecosystem Tech4You "Technologies for climate change adaptation and quality of life improvement", Pilot Project 4.7.1-Open platform "phigital space" (physical and digital) of the type "user profiling" for the advanced and dynamic co-design of interventions on the built and ex novo (Project code: ECS_00000009, CUP: C33C22000290006).

The LIQUEFACT project has received funding from the European Union's Horizon 2020 Research and Innovation Programme under Grant Agreement No. 700748. This support is gratefully acknowledged by the authors.

## CRediT authorship contribution statement

**Daniela Dominica Porcino:** Writing – review & editing, Writing – original draft, Visualization, Validation, Supervision, Resources, Project administration, Methodology, Investigation, Funding acquisition, Conceptualization. **Giuseppe Tomasello:** Writing – review & editing, Writing – original draft, Visualization, Methodology, Investigation, Formal analysis, Data curation, Conceptualization. **Daniela Giretti:** Writing – review & editing, Writing – original draft, Visualization, Validation, Supervision, Methodology, Investigation, Data curation. **Vincenzo Fioravante:** Writing – review & editing, Writing – original draft, Visualization, Validation, Supervision, Resources, Methodology, Investigation.

## Declaration of competing interest

The authors declare that they have no known competing financial interests or personal relationships that could have appeared to influence the work reported in this paper.

## Data availability

Data will be made available on request.

## References

[1] Audemard FA, Gómez JC, Tavera HJ, Orihuela NG. Soil liquefaction during the Arequipa Mw 8.4 June 23, 2001 earthquake, southern coastal Peru. Eng Geol 2005;78(3–4):237–55. https://doi.org/10.1016/j.enggeo.2004.12.007.

[2] Unjoh S, Kaneko M, Kataoka S, Nagaya K, Matsuoka K. Effect of earthquake ground motions on soil liquefaction. Soils Found 2012;52(5):830–41. https://doi.org/10.1016/j.sandf.2012.11.006.

[3] Lirer S, Chiaradonna A, Mele L. Soil Liquefaction: from mechanisms to effects on the built environment. Riv Ital Geotec 2020;3:23–51. https://doi.org/10.19199/2020.3.0557-1405.023.

[4] Ulusay R, Aydan Ö, Kumsar H. Ground liquefaction caused by 6 February 2023 Kahramanmaraş earthquake of Türkiye and some assessments on its extent and impacts on built environment. Bull Eng Geol Environ 2024;83:447. https://doi.org/10.1007/s10064-024-03946-w.

[5] Polito CP, Green RA, Lee J. Pore pressure generation models for sands and silty soils subjected to cyclic loading. J Geotech Geoenviron Eng 2008;143(10):1490–500. https://doi.org/10.1061/(ASCE)1090-0241(2008)134:10(1490.

[6] Seed HB, Martin PP, Lysmer J. The generation and dissipation of pore water pressures during soil liquefaction. In: Report No. UCB/EERC 75-26. USA: report No. UCB/EERC 75-26. Earthquake engineering center. University of California at Berkeley; 1975.

[7] Booker JR, Rahman MS, Seed HB. GADFLEA- A computer program for the analysis of pore pressure generation and dissipation during cyclic or earthquake loading. In: Report No. EERC 76-24 berkeley, California: earthquake engineering center. California at Berkeley: Univ. of; 1976.

[8] Tomasello G, Porcino DD. Influence of sloping ground conditions on cyclic liquefaction behavior of sand under simple shear loading. Soil Dynam Earthq Eng 2022;163:107516. https://doi.org/10.1016/j.soildyn.2022.107516.

[9] Chu M-C, Tsai C-C, Ge L. Excess pore water pressure generation in poorly graded sands with varying particle shapes and relative densities. Soil Dynam Earthq Eng 2024;180:108574. https://doi.org/10.1016/j.soildyn.2024.108574.

[10] Dobry R, Pierce WG, Dyvik R, Thomas GE, Ladd RS. Pore pressure model for cyclic straining of sand. Rensselaer Polytechnic Institute; 1985 [Research report]. Troy, New York: Civil Engineering Department.

[11] Vucetic M, Dobry R. Pore pressure build-up and liquefaction at level sandy sites during earthquakes [Research report CE-86-3]. Troy, NY: dept. of Civil Engineering, Rensselaer Polytechnic Institute; 1986.

[12] Cetin KO, Bilge HT. Cyclic large strain and induced pore pressure models for saturated clean sands. J Geotech Geoenviron Eng 2012;138(3):309–23. https://doi.org/10.1061/(ASCE)GT.1943-5606.0000631.

[13] Berrill JB, Davis RO. Energy dissipation and seismic liquefaction of sands: revised model. Soils Found 1985;25(2):106–18. https://doi.org/10.3208/sandf1972.25.2_106.

[14] Green RA, Mitchell JK, Polito CP. An energy-based excess pore pressure generation model for cohesionless soils. In: Proc.: developments in theoretical geomechanics–the john booker memorial symposium. Sydney, Australia: New South Wales; 2000. p. 383–90.

[15] Jafarian Y, Towhata I, Baziar MH, Noorzad A, Bahmanpour A. Strain energy based evaluation of liquefaction and residual pore water pressure in sands using cyclic torsional shear experiments. Soil Dynam Earthq Eng 2012;35:13–28. https://doi.org/10.1016/j.soildyn.2011.11.006.

[16] Porcino DD, Tomaselo G, Farzalizadeh R. Pore-pressure generation of sands subjected to cyclic simple shear loading: an energy approach. In: Wang L,

Zhang JM, Wang R, editors. Proceedings of the 4th international conference on performance based design in earthquake geotechnical engineering (beijing 2022). PBD-IV 2022. Geotechnical, geological and earthquake engineering. Cham: Springer; 2022. p. 1674–82.
[17] Khashila M, Karray MK, Hussien MN, Ramirez J, Chekired M. Validation of strain/energy-based pore pressure model in one-dimensional response analyses using centrifuge tests. Soil Dynam Earthq Eng 2023;173:108096. https://doi.org/10.1016/j.soildyn.2023.108096.
[18] Elgamal A, Yang Z, Parra E, Ragheb A. Modeling of cyclic mobility in saturated cohesionless soils. Int J Plast 2003;19(6):883–905. https://doi.org/10.1016/S0749-6419(02)00010-4.
[19] Taiebat M, Shahir M, Pak A. Study of pore pressure variation during liquefaction using two constitutive models for sand. Soil Dynam Earthq Eng 2007;27:60–72. https://doi.org/10.1016/j.soildyn.2006.03.004.
[20] Yang M, Taiebat M, Dafalias YF. SANISAND-MSf: a sand plasticity model with memory surface and semifluid state. Geotechnique 2022;72(3):227–46. https://doi.org/10.1680/jgeot.19. 363.
[21] Marcuson WF, Hynes ME, Franklin AG. Evaluation and use of residual strength in seismic safety analysis of embankments. Earthq Spectra 1990;6(3):529–72. https://doi.org/10.1193/1.1585586.
[22] Oda M, Kawamoto K, Sukuzi K, Fujimori H, Sato M. Microstructural interpretation or reliquefaction of saturated granular soils under cyclic loading 2001;127(5):416–23. https://doi.org/10.1061/(ASCE)1090-0241 (2001)127:5 (416).
[23] Chang W, Rathje EM, Stokoe IIKH, Hazirbaba K. In situ pore-pressure generation behaviour of liquefiable sand. J Geotech Geoenviron Eng 2007;133(8):921–31. https://doi.org/10.1061/(ASCE)1090-0241(2007)133:8(921.
[24] Baziar MH, Shahnazari H, Sharafi H. A laboratory study on the pore pressure generation model for Firouzkooh silty sands using hollow torsional test. Int J Civ Eng 2011;9(2):126–34.
[25] Porcino DD, Tomasello G, Diano V. Key factors affecting prediction of seismic pore water pressures in silty sands based on damage parameter. Bull Earthq Eng 2018;16:5801–19. https://doi.org/10.1007/s10518-018-0411-z.
[26] Tomasello G, Porcino DD. Earthquake-induced large deformations and failure mechanisms of silty sands in sloped ground conditions. Soil Dynam Earthq Eng 2023;173:108056. https://doi.org/10.1016/j.soildyn.2023.108056.
[27] Baziar MH, Lashkajani MHM. Prediction of excess pore water pressure generation in sand-silt mixtures during cyclic loading: a dissipated energy-based model. Geotech Geol Eng 2024;42:5209–28. https://doi.org/10.1007/s10706-024-02837-x.
[28] Tomasello G, Porcino DD. Energy-based pore pressure generation models in silty sands under earthquake loading. Geosciences 2024;114:166. https://doi.org/10.3390/geosciences14060166.
[29] Wei X, Yang J, Yang Z-X. Characterizing the liquefaction potential and pore pressure generation of silty sands through the energy-based approach in the framework of critical state soil mechanics. J Geotech Geoenviron Eng 2024;150 (10):04024093. https://doi.org/10.1061/JGGEFK.GTENG-11910.
[30] Mei X, Olson SM, Hashash YMA. Empirical curve-fitting parameters for a porewater pressure generation model for use in 1-D effective stress-based site response analysis. In: Cubrinovski M, editor. Proceedings of the 6th international conference on earthquake geotechnical engineering. New Zealand: New Zealand Geotechnical Society; 2015.
[31] Mele L, Lirer S, Flora A. A simple procedure to calibrate a pore pressure energy-based model from in situ tests. Acta Geotechnica 2022;18:1569–91. https://doi.org/10.1007/s11440-022-01650-1.
[32] Ishihara K, Shimizu K, Yamada Y. Pore water pressures measured in sand deposits during an earthquake. Soils Found 1981;21(4):85–100. https://doi.org/10.3208/sandf1972.21.4_85.
[33] Ishihara K, Muroi T, Towhata I. In-situ pore water pressures and ground motions during the 1987 Chiha-Toho-Oki earthquake. Soils Found 1989;29(4):75–90. https://doi.org/10.3208/sandf1972.29.4_75.
[34] Zimmaro P, Kwak DY, Tsai YT, Stewart JP, Brandenberg SJ, Mikami A, Kataoka S. Database on seismic response of instrumented flood control levees. Earthq Spectra 2020;36(2):924–38. https://doi.org/10.1177/8755293019891712.
[35] Ashford SA, Rollins KM, Lane JD. Blast-induced liquefaction for full-scale foundation testing. J Geotech Geoenviron Eng 2004;130(8):978. https://doi.org/10.1061/(ASCE)1090-0241(2004)130:8(798. 806.
[36] Rollins KM, Amoroso S, Andersen P, Tonni L, Wissmann K. Liquefaction mitigation of silty sands using rammed aggregate piers based on blast-induced liquefaction testing. J Geotech Geoenviron Eng 2021;147(9):04021085. https://doi.org/10.1061/(ASCE)GT.1943-5606.0002563.
[37] Chen Y, Li C, Wang W, Liu H, Yao Y, Ni S, Sarajpoor S. Study on the liquefaction characteristics of saturated sands by millisecond delay blasting. Soil Dynam Earthq Eng 2023;164:107584. https://doi.org/10.1016/j.soildyn.2022.107584.
[38] De Alba PA, Chan CK, Seed HB. Sand liquefaction in large-scale simple shear tests. J Geotech Eng Div 1976;102(9):909–27. https://doi.org/10.1061/AJGEB6.0000322.
[39] Yoshimi Y, Tokimatsu K. Settlement of buildings on saturated sand during earthquake. Soils Found 1977;17(1):23–38. https://doi.org/10.3208/sandf1972.17.23.
[40] Fan Z, Yang Y, Cudmani R, Zhang J, Sun M, Chrisopoulos S. Experimental study on the seismic behavior of tunnels with distinct surface roughness in liquefiable soils. Soil Dynam Earthq Eng 2025;188:109067. https://doi.org/10.1016/j.soildyn.2024.109067.
[41] Lambe PC, Whitman RV. Dynamic centrifugal modeling of a horizontal dry sand layer. Journal of Geotechnical Engineering 1985;111(3):265–87. https://doi.org/10.1061/(ASCE)0733-9410(1985)111:3(265.
[42] Sharp MK, Dobry R, Abdoun T. Centrifuge modelling of liquefaction and lateral spreading of virgin, overconsolidated and pre-shaken sand deposits. Int J Phys Model Geotech 2003;3(2):11–22. https://doi.org/10.1680/ijpmg.2003.030202.
[43] Kutter BL, Manzari MT, Zeghal M. Model tests and numerical simulations of liquefaction and lateral spreading. first ed. Cham: Springer Nature Switzerland; 2017.
[44] Dobry R, El-Sekelly W, Abdoun T. Calibration of non-linear effective stress code for seismic analysis of excess pore pressures and liquefaction in the free field. Soil Dynam Earthq Eng 2018;107:374–89. https://doi.org/10.1016/j.soildyn.2018.01.029.
[45] Giretti D, Fioravante V. Centrifuge modelling of vertical and horizontal drains to mitigate earthquake-induced liquefaction. Geosciences 2023;23:174. https://doi.org/10.3390/geosciences13060174.
[46] Ghassemi A, Seyfi S, Shahir H. Evaluation of variable permeability model in simulation of seismic behavior of uniform level and gently sloping sand layers. Earth Sci Res J 2020;24(3):335–43. https://doi.org/10.15446/esrj.v24n3.60654.
[47] Arulanandan K, Sybico Jr J. Post-liquefaction settlement of sand. In: Houlsby GT, Schofield AN, editors. Proceedings of the Wroth memorial symposium. London, England: Thomas Telfors Ltd; 1992. p. 94–110.
[48] Jafarzadeh F, Yanagisawa E. Settlement of sand models under unidirectional shaking. In: Ishihara K, editor. First international conference on earthquake geotechnical engineering. Rotterdam: Balkema; 1995. p. 693–8.
[49] Shahir H, Pak A, Taiebat M, Jeremić B. Evaluation of variation of permeability in liquefiable soil under earthquake loading. Comput Geotech 2012;40:74–88. https://doi.org/10.1016/j.compgeo.2011.10.003.
[50] Shahir H, Mohammadi-Haji B, Ghassemi A. Employing variable permeability model in numerical simulation of saturated sad behavior under earthquake loading. Comput Geotech 2014;55:211–23. https://doi.org/10.1016/j.compgeo.2013.09.007.
[51] Fioravante V, Giretti D, Airoldi S, Moglie J. Effects of seismic input, fine crust and existing structure on liquefaction from centrifuge model tests. Bull Earthq Eng 2021;19:3807–33. https://doi.org/10.1007/s10518-021-01139-4.
[52] Pervaiz U, Park D, Hashah Y, Xing G. Testing performance of pore pressure models implemented in one-dimensional site response analysis program against centrifuge test data measured in mildly sloping ground. Soil Dynam Earthq Eng 2021;149:106867. https://doi.org/10.1016/j.soildyn.2021.106867.
[53] Hashash YMA, Musgrove MI, Harmon JA, Ilhan O, Xing G, Numanoglu O, Groholski DR, Phillips CA, Park D, Deepsoil. A nonlinear and equivalent linear seismic site response of 1-D soil columns. 2024, V7.1. User manual. Urbana, IL: Board of Trustees of University of Illinois at Urbana-Champaign; 2024 [software], Version 7.1.
[54] Park T, Ahn JK. Accumulated stress based model for prediction of residual pore pressure. In: Delage P, Desrues J, Frank R, Puech A, Schlosser F, editors. Proceedings of the 18th international conference on soil mechanics and geotechnical engineering. Paris: Presses des Ponts; 2013. p. 1567–70.
[55] Park T, Park D, Ahn JK. Pore pressure model based on accumulated stress. Bull Earthq Eng 2015;13:1913–26. https://doi.org/10.1007/s10518-014-9702-1.
[56] Chiaradonna A, Tropeano G, d'Onofrio A, Silvestri F. Development of a simplified model for pore water pressure build-up induced by cyclic loading. Bull Earthq Eng 2018;16:3627–52. https://doi.org/10.1007/s10518-018-0354-4.
[57] Chiaradonna A, Flora A, d'Onofrio A, Bilotta E. A pore water pressure model calibration based on in-situ test results. Soils Found 2020;60(2):327–41. https://doi.org/10.1016/j.sandf.2019.12.010.
[58] Lee MKW, Finn WDL. DESRA-2: dynamic effective stress response analysis of soil deposits with energy transmitting boundary including assessment of liquefaction potential. 38th ed. University of British Columbia; 1978. Vancouver, CB, Canada: Department of Civil Engineering.
[59] Matasović N, Ordonex GA. D-MOD2000 – a computer program for seismic site response analysis of horizontally layered soil deposits, earthfill dams and solid waste landfills (User's Manual). Washington: GeoMotions, LLC: Lacey; 2012.
[60] Dobry R, Ladd RS, Yokel FY, Chung RM, Powell D. Prediction of pore water pressure buildup and liquefaction of sands during earthquakes by the cyclic strain method. National Bureau of Standards Building Science Series 1982;138:150.
[61] Matasović N. Seismic response of composite horizontally-layered soil deposits [Ph.D. Thesis]. Los Angeles: University of California; 1993.
[62] Mei X, Olson SM, Hashash YMA. Empirical porewater pressure generation model parameters in 1-D seismic site response analysis. Soil Dynam Earthq Eng 2018; 114:563–7. https://doi.org/10.1016/j.soildyn.2018.07.011.
[63] Groholski D. Seismic site response analysis and extraction of dynamic soil behavior and pore pressure response from downhole array measurements [Ph. D. Thesis]. University of Illinois at Urbana-Champaign; 2012.
[64] Wilson DW, Boulanger RW, Kutter BL, Abghari A. Aspects of dynamic centrifuge testing of soil-pile-superstructure interaction. Observation and modeling in numerical analysis and model tests in dynamic soil-structure interaction problems. ASCE; 1997. p. 47–63.
[65] Nabili S, Jafarian Y, Baziar MH, Evaluation of the Martin, et al. Pore pressure build up model using laboratory test data. In: Prakash S, editor. Proceedings of the 6th conference of the international conference on case histories in geotechnical engineering, rolla, Missouri: Missouri university of science and technology; 1975. p. 1–8. 2008.
[66] Whitman RV, Dobry R. Modulus and damping for large strains. Soil dynamics (draft). Wiley publishing. Used as course notes for CE1.331 soil dynamics. Spring: MIT; 1993 [Chapter 14].

[67] Kokusho T. Energy-based liquefaction evaluation for induced strain and surface settlement-evaluation steps and case studies. Soil Dynam Earthq Eng 2021;143:106552. https://doi.org/10.1016/j.soildyn.2020.106552.

[68] Towhata I, Ishihara K. Shear work and pore pressure in undrained shear. Soils Found 1985;25(3):73–84. https://doi.org/10.3208/sandf1972.25.3_73.

[69] Liang L. Development of an energy method for evaluating the liquefaction potential of a soil deposit. PhD Dissertation. Department of Civil Engineering. Cleveland, Ohio: Case Western Reserve University; 1995.

[70] Tao M. Case history verification of the energy method to determine the liquefaction potential of soil deposits [ph. D. Thesis]. Department of civil engineering. Cleveland: Case Western Reserve University; 2003.

[71] Baziar MH, Jafarian Y. Assessment of liquefaction triggering using strain energy concept and ANN model: capacity Energy. Soil Dynam Earthq Eng 2007;27:1056–72. https://doi.org/10.1016/j.soildyn.2007.03.007.

[72] Polito C, Green RA, Dillon E, Sohn C. Effect of load shape on relationship between dissipated energy and residual excess pore pressure generation in cyclic triaxial tests. Can Geotech J 2013;50:1118–28. https://doi.org/10.1139/cgj-2012-0379.

[73] Kokusho T, Kaneko Y. Energy evaluation for liquefaction-induced strain of loose sands by harmonic and irregular loading tests. Soil Dynam Earthq Eng 2018;114:362–77. https://doi.org/10.1016/j.soildyn.2018.07.012.

[74] Yang ZX, Pan K. Energy-based approach to quantify cyclic resistance and pore pressure generation in anisotropically consolidated sand. J Mater Civ Eng 2018;30(9):04018203. https://doi.org/10.1061/(ASCE)MT.1943-5533.0002419.

[75] Zhu L, Yang Q, Luo L, Cui S. Pore-water pressure model for carbonate fault materials based on cyclic triaxial tests. Front Earth Sci 2022;10:842765. https://doi.org/10.3389/feart.2022.842765.

[76] Ciardi G, Madiai C. Energy-based assessment of the cyclic behavior of sand stabilized with colloidal silica. J Geotech Geoenviron Eng 2023;149(11):06023005. https://doi.org/10.1061/JGGEFK.GTENG-11612.

[77] Zhang J, Ji X, Zou D, Liu J, Kong X, Zhou C, Fu Y. Study on the energy-based pore pressure model of coarse-grained soils by eliminating membrane compliance. Acta Geotechnica 2023;18:6505–28. https://doi.org/10.1007/s11440-023-02059-0.

[78] Baziar MH, Sharafi H. Assessment of silty sand liquefaction potential using hollow torsional tests— an energy approach. Soil Dynam Earthq Eng 2011;31:857–65. https://doi.org/10.1016/j.soildyn.2010.12.014.

[79] Konstadinou M, Georgiannou VN. Prediction of pore water pressure generation leading to liquefaction under torsional cyclic loading. Soils Found 2014;54(5):993–1005. https://doi.org/10.1016/j.sandf.2014.09.010.

[80] Mei X, Olson SM, Hashash YMA. Evaluation of a simplified soil constitutive model considering the implied strength and porewater pressure generation for 1-D seismic site response. In: Geotechnical frontiers 2017. Orlando, Florida: ASCE; 2017. p. 352–60. https://doi.org/10.1061/9780784480489.035.

[81] Zeng X, Schofield AN. Design and performance of an Equivalent Shear Beam (ESB) model container for earthquake centrifuge modelling. Geotechnique 1996;46(1):83–100.

[82] Brennan AJ, Madabhushi SPG, Houghton NE. Comparing laminar and equivalent shear beam (ESB) containers for dynamic centrifuge modelling. In: Ng CWW, Wang YH, Zhang LM, editors. Proceedings of the sixth international conference on physical modelling in geotechnics. London: CRC Press; 2006. p. 171–6.

[83] Liu L, Dobry R. Seismic response of shallow foundation on liquefiable sand. J Geotech Geoenviron Eng 1997;123(6):557–67. https://doi.org/10.1061/(ASCE)1090-0241(1997)123:6(557.

[84] Adamidis O, Madabhushi SPG. Experimental investigation of drainage during earthquake-induced liquefaction. Geotechnique 2018;68(8):655–65. https://doi.org/10.1680/jgeot.16.P.090.

[85] Porcino D, Caridi G, Malara M, Morabito E. An automated control system for undrained monotonic and cyclic simple shear tests. In: DeGroot DJ, DeJong JT, Frost D, Baise LG, editors. GeoCongress 2006: geotechnical engineering in the information technology age. Atlanta, Georgia, United States: American Society of Civil Engineers; 2006. p. 1–6.

[86] Vaid YP, Sivathayalan S. Static and cyclic liquefaction potential of Fraser Delta sand in simple shear and triaxial tests. Can Geotech J 1996;33(2):281–9. https://doi.org/10.1139/t96-007.

[87] Sivathayalan S, Ha D. Effect of static shear stress on the cyclic resistance of sands in simple shear loading. Can Geotech J 2011;48(10):1471–84. https://doi.org/10.1139/t11-056.

[88] Pan K, Yang ZX. Effect of initial static shear on cyclic resistance and pore pressure generation of saturated sand. Acta Geotech 2018;13:473–87. https://doi.org/10.1007/s11440-017-0614-5.

[89] Finn WDL. Aspects of constant volume cyclic simple shear. In: Khosla V, editor. Advances in the art of testing soils under cyclic conditions, Detroit, Michigan. United States: American Society of Civil Engineers; 1985. p. 74–98.

[90] Dyvik R, Berre T, Lacasse S, Raadim B. Comparison of truly undrained and constant volume direct simple shear tests. Geotechnique 1987;37(1):3–10. https://doi.org/10.1680/geot.1987.37.1.3.

[91] ASTM D8296. Standard test method for consolidated undrained cyclic direct simple shear test under constant volume with load control or displacement control. West Conshohocken, PA, USA: ASTM International; 2019.

[92] Polito CP, Martin JR. Dissipated energy and pore pressure generation patterns in sands and non-plastic silts subjected to cyclic loadings. Geotechnics 2024;4(1):264–84. https://doi.org/10.3390/geotechnics4010014.

[93] Zhou GY, Pan K, Yang ZX. Energy-based assessment of cyclic liquefaction behavior of clean and silty sand under sustained initial stress conditions. Soil Dynam Earthq Eng 2023;164:107609. https://doi.org/10.1016/j.soildyn.2022.107609.

[94] Pan K, Yang ZX. Evaluation of the liquefaction potential of sand under random loading conditions: equivalent approach versus energy-based method. J Earthq Eng 2017;24(1):59–83. https://doi.org/10.1080/13632469.2017.1398693.

[95] Qin Y, Yang Z, Du X, Wu Q, Guoxing C. An energy-based model for the generation of excess pore water pressure in saturated coral sand. Mar Georesour Geotechnol 2023;42(2):193–204. https://doi.org/10.1080/1064119X.2023.2165992.

[96] Jefferies M, Been K. Soil liquefaction: a critical state approach. second ed. New York: Taylor & Francis; 2016.

[97] Dobry R. Liquefaction of soils during earthquakes. Washington, DC: rep. No. CETS-EE-001. NRC: National Research Council; 1985. Committee on Earthquake Engineering.

[98] Terzaghi K. Die berechnung der durchlassigkeitzifer des tones aus dem verlauf der hydrodynamischen spannungserscheinungen. Mathematish-naturwissenschaftliche, Klasse 1923;132(3/4):125–38.

[99] Beber R, Madabhushi SSC, Dobrisan A, Haigh SK, Madabhushi SPG. LEAP GWU 2017: Investigating different methods for verifying the relative density of a centrifuge model. In: McNamara A, Divall S, Goodey R, Taylor N, Stallebrass S, Panchal J, editors. Physical modelling in geotechnics. London: CRC Press; 2018.

[100] Fioravante V. Anisotropy of small strain stiffness of Ticino and Kenya sands from seismic wave propagation measured in triaxial testing. Soils Found 2000;40(4):129142. https://doi.org/10.3208/sandf.40.4_129.

[101] Ueng T-S, Wang Z-F, Chu M-C, Ge L. Laboratory tests for permeability of sand during liquefaction. Soil Dynam Earthq Eng 2017;100:249–56. https://doi.org/10.1016/j.soildyn.2017.05.037.

[102] Matasović N, Vucetic M. Cyclic characterization of liquefiable sands. Journal of Geotechnical Engineering 1993;119(11):1805–22. https://doi.org/10.1061/(ASCE)0733-9410(1993)119:11(1805.

[103] Kondner RL, Zelasko AJS. A hyperbolic stress-strain formulation of sands. In: Proc. 2nd Pan Am. Conf. On soil mech. And found. Engrg. Silo paulo, Brazil: Brazilian association of soil mechanics; 1963. p. 289–324.

[104] Matasović N, Vucetic M. Generalized cyclic-degradation-pore-pressure generation model for clays. Journal of Geotechnical Engineering 1995;121(1):33–42. https://doi.org/10.1061/(ASCE)0733-9410(1995)121:1(33.

[105] Mei X, Olson SM, Hashash YMA. Evaluation of a simplified soil constitutive model considering implied strength and porewater pressure generation for 1-D seismic site response. Can Geotech J 2020;57(7):974–99. https://doi.org/10.1139/cgj-2018-0893.

[106] Ramirez J, Barrero AR, Chen L, Dashti S, Ghograni A, Taiebat M, Arduino P. Site response in a layered liquefiable deposit: evaluation of different numerical tools and methodologies with centrifuge experimental results. J Geotech Geoenviron Eng 2018;144(10):04018073. https://doi.org/10.1061/(ASCE)GT.1943-5606.0001947.

[107] Ziotopoulou K. Seismic response of liquefiable sloping ground: class A and C numerical predictions of centrifuge model responses. Soil Dynam Earthq Eng 2018;113:744–57. https://doi.org/10.1016/j.soildyn.2017.01.038.

[108] Zeghal M, Elgamal A-W, Tang HT, Stepp JC. Lotung downhole array. II: evaluation of soil nonlinear properties. Journal of Geotechnical Engineering 1995;121(4):363–78.

[109] Dash HK, Sitharam TG. Undrained cyclic pore pressure response of sand-silt mixtures: effect of nonplastic fines and other parameters. Geotech Geol Eng 2009;27:501–17. https://doi.org/10.1007/s10706-009-9252-5.